Rheological conditions for emplacement of Ural-Alaskan-type ultramafic complexes

Laurent Guillou-Frottier, Evgenii E.B. Burov, Thierry Augé, Eric Gloaguen

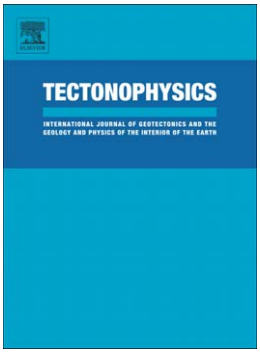

Rheological conditions for emplacement of Ural-Alaskan-type ultramafic complexes

Laurent Guillou-Frottier, Evgueni Burov, Thierry Augé, Eric Gloaguen

PII: S0040-1951(14)00087-0
DOI: doi: 10.1016/j.tecto.2014.02.002
Reference: TECTO 126203

To appear in: *Tectonophysics*

Received date: 4 October 2013
Revised date: 29 January 2014
Accepted date: 2 February 2014

Please cite this article as: Guillou-Frottier, Laurent, Burov, Evgueni, Augé, Thierry, Gloaguen, Eric, Rheological conditions for emplacement of Ural-Alaskan-type ultramafic complexes, *Tectonophysics* (2014), doi: 10.1016/j.tecto.2014.02.002

Rheological conditions for emplacement of Ural-Alaskan-type ultramafic complexes

Laurent GUILLOU-FROTTIER [a,*], Evgueni BUROV [b, c], Thierry AUGÉ [a] and Eric GLOAGUEN [a]

a : Bureau de Recherches Géologiques et Minières, BRGM, ISTO, UMR 7327, Orléans, France

b : UPMC Sorbonne Universités, ISTEP, UMR 7193, Université Pierre et Marie Curie, F-75005, Paris, France

c: CNRS, ISTEP, UMR 7193, F-75005, Paris, France.

Revised manuscript submitted to *Tectonophysics*, January 29th, 2014

Special Volume "*Observational and Modelling perspectives on the Mechanical properties of the Lithosphere*"

(*) Corresponding author: Laurent GUILLOU-FROTTIER, BRGM, Georesources Division, 3 av. C. Guillemin, BP 36009, 45060 Orléans Cedex 2, France; tel: +33 238 644 791; fax: +33 238 643 554; l.guillou-frottier@brgm.fr

Abstract

Ural-Alaskan- (or Alaskan-) type complexes correspond to a particular class of ultramafic intrusions that attract particular attention due to their deep mantle origin and their platinum-group element (PGE) mineralization. When defined as massifs of dunite-clinopyroxenite, only forty-six complexes are reported in the literature. These large-scale dunite pipe-like structures are rarely isolated and they even can appear in clusters. To better understand genesis of these relatively young (< 460 Ma) complexes, a worldwide compilation has been built, and three categories have been defined: single circular or elliptical bodies, twin bodies with similar shapes, and dismembered dunite bodies. PGE enrichment in Alaskan-type complexes is highest for the second category, where twin bodies are interpreted as horizontal sections of Y-shaped dunite pipes. To constrain mechanical properties of the lithosphere allowing emplacement of the Alaskan-type complexes, the forceful diapiric ascent hypothesis is investigated through numerical thermo-mechanical models. One hundred high resolution experiments accounting for realistic phase changes and softening mechanisms have been performed. The experiments show that with no rheological softening of the host rock and in case of a relatively weak ductile lower crust, the uprising magma tends to spread laterally without reaching the surface. To account for the forceful ascent of deep magmas, it is hence necessary to assume a strong lower crust rheology and strong local softening mechanisms. Besides reproducing the clustered distribution of the weakness zones representing magma pathways, these latter experiments reproduce large-scale pipe-like (cylindrical) structures, Y-shaped and funnel-shaped bodies, and laterally-shifted structures. Interestingly, zones of highest strain rates are located at the bottom parts of the inclined edges of Y-shaped and funnel-shaped bodies. The restricted age range of Alaskan-type complexes (< 460 Ma) would mean that prior to this time, the lower crust was less resistant due to the hotter geotherm, prohibiting the possibility of “Alaskan-type magmatism”.

Keywords: Ural-Alaskan complexes; Dunite core geometry; Magma ascent mechanisms; Platinum-group elements; Numerical modelling; Rheology; Softening

1. Introduction

Alaskan-type (or Ural-Alaskan-type) complexes represent a group of ultramafic bodies where orthopyroxene is generally absent, and can thus be described as dunite-clinopyroxenite massifs. They have been originally defined as intrusions of olivine-rich lithologies (considered as mantle-derived material) with a concentrically zoned distribution, evolving from a dunite core to a clinopyroxenite rim, with gabbros or diorites at the margins (Taylor, 1967). The size of Alaskan-type complexes ranges from a few to hundreds of km², with one exception, the Guli massif, reaching 2000 km². In map view, they present circular or elliptical geometries, and can appear as isolated bodies or accompanied by a twin body of similar size, each of them being separated by a few kilometres. At a larger scale (hundreds of kilometres), several Alaskan-type bodies can be gathered in clusters, like in the Urals or in south-eastern Alaska (Figure 1). Although ultramafic rocks of various typologies can be found in many places on Earth, Alaskan-type complexes are very scarce since only 46 complexes can really fit the above definition of a dunite core surrounded by a clinopyroxenite rim (Table 1). Twelve other ultramafic bodies were classified in the past as Alaskan-type complexes but they do not include a dunite core, and hence they are not listed in Table 1 (e.g. Turn Mountain, Salt Chuck and Sukkwan Island ultramafic bodies in SE Alaska, Himmelberg and Loney, 1995). There is also no evidence for a dunite core in the so-called Alaskan-type complexes of Gnat Lake or Menard Creek ultramafic bodies in British Columbia (Nixon et al., 1997). Similarly, although Pettigrew and Hattori (2006) suggested that the Neo-Archean ultramafic intrusions in the Quetico subprovince, Canada, correspond to Alaskan-type complexes, it appears that their cores are made of wehrlite (less than 90% of olivine) and not of dunite. Nevertheless, even if the listed number of Alaskan-type complexes depends on their definition and on the interpretation of geological maps, their scarcity is noteworthily evident. Besides their scarcity, dunite-clinopyroxenite massifs show another intriguing feature, dealing with their ages: Alaskan-type complexes were emplaced during a small part of the Earth history, from 460 to 20 Ma.

Ultramafic bodies and Alaskan-type complexes in particular, have been studied for a long time because of their associated mineralization in platinum-group elements (PGE) (Johan, 2002). Platinum-Group Elements, which refer to six metals (osmium, iridium, ruthenium, rhodium, platinum and palladium), have become essential to modern industry and are now classified as “strategic” metals. Among these elements, two of them, iridium and platinum, are particularly present in Alaskan-type bodies, and it appears that the price of these two metals has been continuously increasing for the last decade. However, the number of exploited PGE ore deposits is largely limited to South Africa (Bushveld complex) and Russia (Noril’sk intrusion). In addition, the principal source of PGE in Alaskan-type complexes is placer deposit and not primary mineralization. This partly explains that there are only few studies dedicated to the emplacement mechanisms of Alaskan-type complexes which could help understand the conditions of PGE mineralization.

Platinum “nuggets” have been discovered and exploited within placers spatially associated with Alaskan-type bodies (e.g. Slansky et al., 1991; Tolstykh et al., 2000; Malitch et al., 2002; Barkov et al., 2005). Placers remain an important source for PGE production in Russia, after the Ni-Cu sulfides ores of Noril’sk-type intrusions (Johan, 2002; Malitch and Thalhammer, 2002). According to Thakurta et al. (2008) who studied the Alaskan-type Duke Island complex, southeastern Alaska, “*the potential for the occurrence of world-class Cu-Ni-PGE sulphide deposits in Alaskan-type complexes should not be overlooked*”. Although some authors consider the absence of sulphides as representative of Alaskan-type bodies (e.g. Johan, 2002), this feature is not retained in our definition (a dunite core surrounded by clinopyroxenites).

Another recent study (Nazimova et al., 2011) emphasized on the important platinum mineralization of the Galmoenan massif, Kamchatka, possibly defining, in addition to its well-known placer deposits, an economic, medium-size platinum deposit of primary type. Two hundred kilometres southwest of the Galmoenan complex, numerous platinum “nuggets” were also found in placers from the Pustaya River, which crosses the Koryak-Kamchatka platinum belt related to eroded Alaskan-type intrusions (Tolstykh et al., 2000). It must be

stressed that placers around Alaskan-type bodies are not the sole type of PGE mineralization. Indeed, several examples have shown that primary type mineralization, where PGE are associated with chromitite lenses within dunites, have been exploited in the past (e.g. Nizhny Tagil, Augé et al., 2005), but their contribution remains historically very low compared to placer production. However, chromite-bearing dunites within restricted parts of the dunite cores appear to represent a potential economic target (e.g. Galmoenan, Nazimova et al., 2011).

Often associated with the location of ancient subduction zones (Urals, Alaska, British Columbia, Kamchatka, Colombia), Alaskan-type complexes can also form in intracontinental settings (Siberia, Ethiopia, Far East Russia). Several mechanisms have been invoked to explain the ascent and emplacement of mantle-derived magmas at the Earth's surface. Melting from mantle plume heads or from subduction settings have both been proposed. Although Alaskan-type complexes are not necessarily linked to subduction, they are still considered by some researchers as geological imprints of past subduction zones (e.g. Su et al., 2012). On the contrary, Sutherland (1998) suggested a plume model where magmatic diapirs derived from the plume head rise in zones of increasing tensional stress, creating "tube-like" intrusions (see also Burg et al., 1998; Pirajno et al., 2008). Studying ascent mechanisms of ultramafic bodies, Gerya and Burg (2007) and Burg et al. (2009) found that large-scale geodynamic processes are not necessarily required, and that local rheological properties could lead to "translithospheric diapirism", a mechanism with which mantle-derived material could quickly rise up through the lithospheric mantle and the crust. In particular, a cold elasto-plastic crust would facilitate the upward propagation through the crust. This process was initially suggested by Bodinier et al (2002), who analysed microstructural, geochemical and mineralogical data from dunite and pyroxenites of the Kondyor complex. The authors concluded from previous gravimetric data and tectonic reconstructions that the massif represents "*an apex of a dense ultramafic cylinder rooted down to, at least, 10 km depth*". Magma at the origin of the Kondyor dunite would have accumulated at the base of the lithospheric mantle, triggering a forcefully ascent of a solid-state dunite diapir. Here and

in the following, the “solid-state” ascent refers to the rheological behaviour of mantle-derived material, which corresponds to partially molten peridotite with a low density but a high effective viscosity.

The present study consists in looking for appropriate rheological conditions allowing simulations of magmatic processes at the origin of Alaskan-type complexes (fast ascent through the entire lithosphere, particular geometries at the surface, clustering process), through lithospheric-scale thermo-mechanical models that account for the properties of the involved magma. Realistic rheological laws for the crust and the lithosphere (see Supplementary material), as well as realistic phase changes, have been included in the thermo-mechanical numerical model. In particular, our numerical results focus on spatial distribution and geometries of the weakness zones that are created by the ascent of a deep and hot mafic magma.

2. Alaskan-type complexes: general description and classification

Alaskan-type complexes are defined by the following successive events: : first a dunite core is emplaced; second, melt-rock reactions develop successively rims of wehrlite, followed by clinopyroxenites ± hornblendite and then monzonite-gabbro (i.e. absence of orthopyroxene); the contacts between ultramafic and surrounding gabbroic rocks are sharp; the chemical composition of olivine in dunites is highly magnesian; chromite is a phase occurring exclusively in dunite, where it is ubiquitous and locally forms concentration occurring as schlieren or pseudo-layers enriched in PGE (see Johan, 2002 for a detailed review). Ultramafic and mafic rocks contain significant proportions of hydrated minerals (amphibole, phlogopite) and hydrated bodies (ultramafic-mafic pegmatoids). Additional common features to Alaskan-type complexes were later suggested, like the specific concentration and distribution of rare-earth elements (REE) in ultramafic and gabbroic rocks, or the relative absence of sulphides (see Johan, 2002). In the following, we present a distinct classification, based on pure geometrical considerations.

2.1 Surface expression

When geological maps of Alaskan-type complexes are examined, three distinct classes based on surface geometries can be defined, regardless of the geodynamic setting (Figure 2). The first category includes circular or elliptical surface expression of dunite and clinopyroxenite rims with an external diameter of several kilometres (Figure 2a). For some cases, more elongated shapes are observed (e.g. Yubdo, Gaositai, Nizhny Tagil, Wrede Creek, Figure 2c). The second category corresponds to twin bodies (similar shape and size), showing dunite cores of several kilometres in size separated by a few kilometres, each of them being surrounded by clinopyroxenites (e.g. Galmoenan, Goodnews Bay and Duke Island in Figure 2b; Kachkanar, Owendale and Condoto in Figure 2d). The third category includes disconnected dunite blocks of different sizes (e.g. Lunar Creek and Uktus, Figure 2d). All the other Alaskan-type complexes not shown in Figure 2 but listed in Table 1 can be classified in one of the three categories. For example, geological maps of the Turnagain, Red Bluff or Kane Peak ultramafic bodies (Himmelberg and Loney, 1995; Scheel et al., 2009) clearly indicate that they belong to the first category of Alaskan-type complexes. In British Columbia, the Polaris complex belongs to the second category since it comprises two main dunite cores separated by wehrlite and clinopyroxenite (Nixon et al., 1997). Third column of Table 1 indicates which category the Alaskan-type complex belongs to, with the number of dunite cores (one, two or several), when available.

2.2 Vertical models

As mentioned above, gravity measurements around the Kondyor massif led Efimov and Tavlin (1978) to suggest that ultramafic rocks extend as a cylindrical pipe down to a depth of at least 10 km. Interpretations of geological data at Union Bay, southeastern Alaska, by Ruckmick and Noble (1959) and Himmelberg and Loney (1995) suggest that ultramafic rocks delineate an almost vertical pipe with slightly decreasing diameter with depth (funnel-shaped pipe). Again, based on geological observations, van der Poel and Hinderman (2000) described the two twin bodies of the Goodnews Bay complex as vertical pipes widening out at the surface. Recently, the geometric model of the Duke Island complex proposed by Thakurta et al. (2008), which was derived from a previous model by Butler et al. (2001),

illustrates a three-branches structure, two of which including dunite pipes surrounded by clinopyroxenites, joining at depth and forming a common “trunk”. To summarize, vertical structure of Alaskan-type complexes would correspond to magmatic conduits (pipes) which could have pierced the mantle lithosphere and the crust through a diapirism mechanism (Bodinier et al., 2002; Gerya and Burg, 2007; Burg et al., 2009).

2.3 Clusters

Clustering of Alaskan-type complexes (Figure 1b) can be quantified by the averaged distance between nearest neighbours, which is around 60 km for the Urals, and around 30 km for south-eastern Alaska. For both cases, the role of past or present subduction zones has been invoked (Murray, 1972). Actually, there is no reason to get same values since volcanism related to subduction seems to be randomly distributed (de Brémond d’Ars et al., 1995). According to these authors, spatial distribution of subduction-related volcanoes would be representative of melting conditions and deep magmatic activity, such as recurrent magmatic pulses.

Clustering of Alaskan-type complexes is not necessarily linear (like in the Urals, Figure 1) and several neighbouring bodies seem to have been emplaced in a single event (see in Table 1 the ages of Alaskan-type complexes in the Urals, in Kamchatka, and in SE Alaska). Simultaneous emplacement of such deep magmatic bodies probably requires a particular thermo-mechanical event affecting the bulk crust over several hundreds of km.

Uprising of mantle-derived material through the lithosphere requires the development of weak crustal zones. The clustering phenomenon (of weak zones) might be analogous to the faulting spatial periodicity problem. Fracturing and faulting spatial periodicity has been extensively studied in the past decades (e.g. Ouillon et al., 1996). These authors concluded that faulting spatial periodicity is mainly controlled by rheological layering of the crust and not by the complex rupture process. Similarly, it is the rheology of the lower crust which appears to control folding of the lithosphere (Gerbault et al., 1999). In the following sections, the clustering of Alaskan-type complexes is investigated through distinct possible crustal rheologies.

3. Physical properties of ultramafic rocks and magmas

Physical properties of olivine-rich ultramafic rocks (density, thermal properties, and rheology) have been studied by several teams in the past (Chopra and Paterson, 1981, 1984; Chopra, 1997; Mei and Kohlstedt, 2000a, 2000b; Suzuki and Ohtani, 2003; Gibert et al., 2005; Wang, 2010; Keefner et al., 2011). Recently obtained data on clinopyroxene crystals from the Konder and Inagli massifs have shown a close composition and a similar configuration of REE patterns to those obtained with samples from the Alaskan-type Kytlym and Nizhni Tagil massifs (Simonov et al., 2011). The authors concluded that dunites of the Konder and Inagli massifs were produced by water-rich (up to 0.6%) magmas at temperatures of 1300-1460°C. This is in accordance with the amount of hydrated minerals (amphibole, phlogopite) and hydrated bodies (ultramafic-mafic pegmatoids) observed in such Alaskan-type complexes.

It is well-known that the presence of water strongly modifies rheological properties, and such hydrated magmas at high temperature may indeed undergo unexpected flow regimes. The presence of water in olivine rich magmas also induces a decrease in viscosity: a reduction factor of 4 to 10 should be applied to mantle-derived material if viscosity of mid-oceanic ridge basalts had to be used (Mei and Kohlstedt, 2000b). Laboratory experiments attempting to reproduce realistic thermal and mechanical conditions are however limited. As emphasized by Korenaga and Karato (2008), olivine rheology is complex since a minimum of eighteen parameters are required to write rheological laws. In addition, rheological laws for water-rich olivine suffer major uncertainties, as it is actually the case for crustal rocks (Burov, 2007). Recently, high-pressure and high-temperature experiments on deformation of dunite demonstrated that accounting for the role of oxygen fugacity in the range of upper mantle conditions, could decrease dunite viscosity by a factor of ~5 (Keefner et al., 2011). Korenaga and Karato (2008) illustrate different effective viscosity profiles for the upper 300 km of the mantle, for dry and wet cases and for different chosen geotherms; all viscosity profiles for

wet conditions show uncertainties of several orders of magnitude. The authors particularly insist on the large scatter of experimental data under wet conditions.

As far as thermal properties are concerned, it seems that they can be underestimated when experimental data are considered. Gibert et al (2005) concluded from their measurements that thermal diffusivity of mantle-derived material could be 50% higher than previously assumed. It follows that heat transfer processes related to low viscous olivine-rich rocks at high temperatures could thus be much more efficient, and thus much faster than commonly thought.

All the above-mentioned experimental data suggest that olivine-rich mantle rocks at high temperature may exhibit particular rheological behaviour involving strong strain and/or strain-rate softening mechanisms (see also Burov, 2011). As far as modelling parameters are concerned, density is here determined from mineralogical phases defined by ambient thermo-mechanical conditions (pressure and temperature) through equations of state derived for corresponding mineralogical compositions (see below). The effective viscosity is assessed from rock mechanics data on flow law parameters for given thermo-mechanical conditions, together with testing parameters of softening rules defining local strain-induced reduction in viscosity (see next section). Thus, the rheological model comprises distinct softening rules that are tested until a reasonable translithospheric diapirism mechanism is achieved.

4. Numerical model and preliminary tests

In the following, we present a series of numerical experiments aimed at reproducing the apparent “lithospheric diapirism” which is assumed to explain the ascent and emplacement mechanisms of Alaskan-type complexes. Main model features and tests experiments are first presented (Figure 3). Then, the results obtained with specific softening rules allowing the reproduction of typical geometries of Alaskan-type bodies are discussed.

4.1 Model features

We basically follow the philosophy of the earlier study by Gerya and Burg (2007), yet for a wider range of thermo-tectonic conditions, rheological assumptions and configurations specific to Alaskan-type complexes. We also test different softening rules and other parameters in order to assess the rheological properties of the lithosphere enabling for magma ascent from great depth. On the technical side, the main difference of our approach from that of the one developed in Gerya and Burg (2007) refers to a formally higher degree of physical consistency achieved through direct implementation of free surface, viscous-elastic-plastic rheology and phase changes (the two latter features were also integrated in the latest versions of the code by T. Gerya but were not applied to the problem of intrusion of ultramafic magmatic bodies). In particular, incorporation of continuous phase changes (Burov and Yamato, 2008) implies that rock density is thermo-dynamically consistent being dynamically updated as function of P-T (pressure and temperature) conditions from the equations of state ρ = *f(P,T)* based on minimization of Gibbs free energy for given mineralogical composition. With that goal, the thermodynamic algorithm PERPLEX and its data base (Connolly, 2005) have been coupled with the main code. This approach not only provides more reliable values for density and for hence thermodynamically consistent definitions of thermal expansion α (*P,T*) and compressibility β (*P,T*), but also for thermal and elastic parameters, the amount of released or absorbed fluids and other physical properties that can be used for thermo-mechanical calculations and on post-processing stage. As mentioned above, PERPLEX minimizes free Gibbs energy *G* for a given chemical composition to calculate an equilibrium mineralogical assemblage for given P-T conditions:

$$G = \sum_{i=1}^{n} \mu_i N_i \qquad (1)$$

where μ_i is the chemical potential and N_i the moles number for each component i constitutive of the assemblage. Given the mineralogical composition, the computation of density is then straightforward (e.g., Yamato et al., 2007; Burov and Yamato, 2008). Thermal expansion α_{eff} is corrected for latent heat following Gerya and Burg (2007):

$$\alpha_{eff} = \alpha(P,T) + \rho_0 \frac{Q_L}{T}\left(\frac{\partial M}{\partial p}\right)_T \quad (2)$$

where ρ_0, Q_L, M, T and p are density, latent heat of melt, volume fraction of melt, temperature and pressure, respectively. To solve the thermo-mechanical part of the problem, we use the code Flamar 12 (outgrowth of FLAC and Paravoz (Cundall, 1989; Poliakov et al., 1993)). Flamar is a well-tested code that have been used for many geodynamic applications including exhumation of metamorphic domes (Tirel et al., 2008), mantle-lithosphere interactions (d'Acremont et al., 2003; Burov and Cloetingh, 2009), continental collision (e.g., Toussaint et al., 2004; Burov and Yamato, 2008) and metamorphic rock exhumation (e.g., Burov et al., 2012). As its predecessors, Flamar is a large strain fully explicit time-marching algorithm that locally solves full Newtonian equations of motion in a continuum mechanics approximation:

$$\langle \rho \ddot{\mathbf{u}} \rangle - \nabla \boldsymbol{\sigma} - \rho \mathbf{g} = 0 \quad (3)$$

coupled with viscous-elastic-plastic constitutive equations (see Supplementary material):

$$\frac{D\sigma}{Dt} = F(\sigma, \mathbf{u}, \dot{\mathbf{u}}, \nabla \dot{\mathbf{u}}, ...T...) \quad (4)$$

with equations of heat transfer and with state equations:

$$\rho\, C_p\, DT/Dt - \nabla(k\, \nabla T) - H = 0 \quad (5)$$

$$\rho = f\,(P,T) \quad (6)$$

Here $\mathbf{u}$, $\boldsymbol{\sigma}$, $\boldsymbol{g}$, k are the respective terms for displacement, stress, acceleration due to body forces and thermal conductivity; dot represents the time-derivative; pressure P is negative for compression. In the eq. 5, heat advection term $\dot{\mathbf{u}}\nabla T$ is included in the Lagrangian derivative DT/Dt. The triangular brackets in (3) specify conditional use of the related term as in quasi-static mode inertial terms are damped using inertial mass scaling (Cundall, 1989). The terms t, C_p, H designate respectively time, specific heat, and internal heat production (radiogenic heating, shear heating, latent heat). The expression $\rho = f(P,T)$ refers to the density computed

by a thermodynamic module PERPLEX as function of P and T. The terms $D\sigma/Dt$ and F are the objective Jaumann stress time derivative and a functional, respectively. In the Lagrangian method, incremental displacements are added to the grid coordinates allowing the mesh to move and deform with the material. This allows for the solution of large-strain problems while using locally the small-strain formulation: on each time step the solution is obtained in local coordinates, which are then updated in a large strain mode.

Solution of (3) provides velocities at mesh points used for computation of element strains and of heat advection $\dot{\mathbf{u}}\nabla T$. These strains are used in (4) to calculate element stresses and equivalent forces used to compute velocities for the next time step. Due to the explicit approach, there are no convergence issues, which is rather common for implicit methods in case of non-linear rheologies. The algorithm automatically checks and adopts the internal time step using 0.1 – 0.5 of Courant's criterion of stability, which warrants stable solution.

4.2. Model setup and test experiments

We first run a series of experiments roughly following the strategy chosen by Gerya and Burg (2007), yet for conditions and parameters compatible with the Alaskan-type complexes. The setup of the models is following:

In the reference model, the computational domain is 1000 km wide and 300 km deep with a homogeneous grid comprising 600 x 260 rectangular elements. Some experiments were run using local mesh refinement allowing for higher spatial resolution in center of the model (0.8 km x 0.5 km). Depending on the experiment, the lithosphere was either 100 km or 200 km thick including 40 km thick crust. Semi-spherical 200 km (in some experiments 50 km or 100 km) wide magmatic source is placed at the bottom of the model. An initially narrow – 2 element wide – dike-like conduit connects the source region with the bottom of the crust (dashed white contour in Figure 3a). Density and viscosity contrasts impose large and fast modifications in the lithospheric and crustal stress regimes; thermo-mechanical evolution of the system is thus computed until high strain rates are achieved at the surface. Composition,

stress, strain and strain rates are computed for each grid cell, but “magma flow” (in terms of fluid dynamics) is not simulated in these experiments due to their time scales. The conduit is initially blocked at Moho depth to investigate further initialization of the potential magma pathways in the overlying crust. We do not continue experiments once the pathways are initialized since further propagation of magma and its interaction with the walls of the pathways are beyond the scope of this study, requiring a separate parametric investigation at local scale. The following illustrations show compositional fields and strain rate values that are computed after thousands years of evolution. In particular, large values of strain rates are assumed to be located where contrasts in physical properties are the highests. In other words, the terms “magma ascent” in the following text correspond to the upward migration of high strain rate zones.

In the reference experiments (Figure 3b and 3c) we have made a conventional assumption on the strength profile of the background lithosphere assuming initial geotherm yielding 60-70 mW/m² at surface (thermotectonic age of 100 Ma), granite-dominated crust, quartz-diorite lower crust and dry olivine mantle, and no ductile softening. We hence use olivine rheological parameters for mantle and quartz-granite rheology for the crust (see Supplementary material). The upper boundary condition is free surface, the bottom condition corresponds to Winkler basement (hydrostatic), and the lateral conditions are zero horizontal velocities. The thermal boundary conditions are zero temperature at surface, 1400°C at the bottom of the model (300 km depth), and zero lateral outflows. The phase changes are computed for the following compositions: mantle – peridotite; crust – granite; magma – partially molten peridotite.

4.2.1 The influence of compositional density contrast.

The density of partially molten magma is subject to large variations that depend on composition, transient P-T conditions and fluid content. We thus first tested end-member cases with various density contrast cut-offs (as defined by $(\rho_m-\rho_b)/\rho_b$, where ρ_m is magma density and ρ_b the background rock density): from 0.1 to 0.5. In these experiments we did not

activate thermodynamic phase changes. These experiments show the extreme importance of the density contrast on magma emplacement and ascent rate (see Figure 3b, where density contrast between the magma and the mantle equals 0.4 and 0.2). It is important to note that magma ascent velocity is extremely high, reaching several tens to hundreds of m/yr. These values are in accordance with estimates from previous analytical and numerical studies that account for realistic (non-Newtonian) rheologies (e.g. Weingerg and Podladchikov, 1994; van Keken, 1997; Burov et al., 2003).

4.2.2 Experiments with thermodynamically consistent densities

The next series of reference experiments have been implemented with thermodynamically consistent account for phase changes (Figure 3c). Due to P-T dependent density, surface impact of magma is moderate compared to the previous models with fixed density contrast; a relatively large secondary magma region forms at the base of the crust, sourcing magma propagation to the surface. One can observe, similarly to the experiments of Gerya and Burg (2007), that magma ascent creates a deviatoric stress field provoking brittle faulting at surface. The created faults go deep down to 40 km depth and thus may serve for channeling magma to the surface. It is noteworthy that formation of surface faults is conditioned by 2 major factors: (1) the assumed crustal geotherm and (2) magma viscosity cut-off. The background geotherm should be relatively cold in the crustal region to make brittle deformation possible while magma should not be neither too viscous nor too fluid: its viscosity must be lower than 10^{18} Pa.s, otherwise its ascent will be too slow and magma would be stalled at some depth, but greater than 10^{15} Pa.s, otherwise magma might spread laterally somewhere in the crust instead of pushing the brittle crust up. These high viscosity values are one order of magnitude higher than those used by Gerya and Burg (2007), where the associated melt fraction was around 10 to 30% vol. However, in case of the presence of external extensional field (tectonic extension), faults may be formed even in cases where the above conditions are not satisfied (see an example in Burov and Guillou-Frottier, 1999).

5. Experiments with softening mechanisms

As can be seen from the experiments of the previous sections, the reference thermo-rheological structure results in relatively weak ductile lower crust, so that magmatic material ascending from the chamber spreads laterally at some level within the ductile lower crustal layer resulting in distributed deformation at surface since it is denser than the normal crust. It follows that the magmatic conduit is destroyed in its crustal part.

For these reasons, further series of high resolution experiments tempted to find the rheological conditions under which the magmatic material can mechanically reach the uppermost crustal layers without destroying the integrity of the magmatic conduit. The major parameters that have been tested within these experiments were: (1) the lower crustal rheology; (2) mantle rheology and geotherm; (3) softening mechanisms in the brittle and ductile parts; (4) width of the magmatic conduit; (5) magma temperature.

Without detailing all experiments of this sensitivity study, we have found that preservation of the magmatic channel requires strong lower crustal rheology ("diabase/granulite") and strong "aggressive" softening of the brittle and ductile material. We have also extended the brittle failure criterion by adding to the common Mohr-Coulomb criterion that operates under overall compression (i.e. negative pressure, $P < 0$), the parabolic Griffith's criterion applicable in pure tension (positive pressure, $P > 0$):

$$\tau^2 = 4T_0^{\,2} + 4T_0\sigma_n \qquad (7)$$

where τ is shear stress, T_0 is tension cut-off, typically 20-40 MPa, σ_n is normal stress. The Griffith failure can be controlled by varying T_0 ($T_0 = 0$ means permanent failure, $T_0 = 1000$ MPa means practically no tensile fracturing). As mentioned, this criterion applies when pressure becomes positive, in case of dilatation, basically in the uppermost rock layers (first kilometers in depth) where tensile stresses created by magma upraise and upward bending of the uppermost layers can negate lithostatic compressive pressure due to rock weight. Created tensile faults are "mode I" faults, i.e. these faults are normal to the tension axis while the Mohr-Coulomb faults are "mode II" faults. In deeper rocks total pressure is practically

always negative due to the rapidly growing weight of the rock column (about 25-30 MPa per km), so Mohr-Coulomb failure prevails.

The experiments detailed below show representative cases in which magmatic material arrives to break through the brittle crust and find its way to the surface. The series of experiments demonstrate the effects of different strain softening mechanisms in the ductile part. For the brittle part, we use linear cohesion softening, where cohesion drops from 20 MPa to 0 in the strain interval between 0.1 and 0.5. The used softening laws account for cumulative effects of grain size reduction, variations in fluid content in the deforming rock, partial melting and other effects mentioned in the previous sections. It is noteworthy that the choice of the form of the softening rule basically has no quantifiable experimental justification due to multiple processes involved. For example, Huismans and Beaumont (2003) assumed aggressive softening for the brittle and brittle rock assuming similar relations to show that the observed morphologies of rifted basins cannot be explained without frictional-plastic and viscous strain softening. Similarly, Gerya and Burg (2007) and most other workers assumed softening laws that basically do not stem from experimental rock mechanics but from field observations and thermo-mechanical models that show that at macroscopic scale faults and shear bands should undergo strong softening to explain the observed strain patterns and evolution of geological structures. In general, linear strain-softening laws (e.g., Huismans and Beaumont, 2003) are used and we here follow the same approach by implementing a simple piecewise linear ductile softening rule:

$$\text{if } \varepsilon \le \varepsilon_0, \qquad \mu(\varepsilon) = \mu(T,\sigma,\dot{\varepsilon}\ \ldots) \tag{8}$$

$$\text{if } \varepsilon_1 > \varepsilon > \varepsilon_0, \qquad \mu(\varepsilon) = \mu\,(1 - \lambda(\varepsilon-\varepsilon_0)/(\varepsilon_1-\varepsilon_0)) \tag{9}$$

$$\text{if } \varepsilon \ge \varepsilon_1, \qquad \mu(\varepsilon) = \mu\,(1-\lambda) \tag{10}$$

where ε_0 and ε_1 are respectively minimal and maximal accumulated strain values, within which progressive softening is applied; μ is effective initial viscosity derived as function of T, σ, $\dot{\varepsilon}$ and material parameters; λ is a constant viscosity factor such that $(1-\lambda)$ is maximal ratio between viscosity after and before softening, e.g., λ = 0.99900 means 3 order maximal

reduction of viscosity. We changed ε_0 from 0.1 to 0.2, ε_1 from 0.5 to 2.0 and λ from 0.90000 to 0.99999. Seven particularly remarkable cases are detailed below.

5.1 Case 1.

The experiment shown in Figure 4 corresponds to $\varepsilon_0 = 0.2$, $\varepsilon_1 = 0.5$, $\lambda = 0.99900$. This experiment clearly shows that the ascending magma has widened the initially thin channel (Figure 4a). Before arriving at the base of the crust, fractures – or weakness zones – developed at several locations, as it can be seen in the strain rate pattern of Figure 4b, which also shows localization of ductile strain near channel walls that are mechanically eroded during magma ascent. Note in Figure 4c that the surface uplift extends over a distance greater than 100 km, and that spacing between crustal channels of high strain rates equals, respectively, 42, 23, 10, 20, 15 and 15 km (av. 20 ± 10 km).

An additional peculiar feature is revealed in Figure 4b: some zones of high strain rate values in the crust (light green and yellow zones) exhibit a triangular configuration, or funnel-shape geometry. In addition, over the 8 fractured (weakness) zones, only one appears with an angle (laterally shifted body at shallow depths), the others being mostly vertical. Interestingly, 4 of them are not directly connected to the magmatic channel. These observations are consistent with several characteristics of the previously described Alaskan-type complexes, like the clustering phenomenon (see also discussion). Figure 4c illustrates the topography evolution, where fractures/channels are characterized by local subsidence, which is not visible at early stages. The large-scale doming begins to appear at ~0.5 kyr and clearly develops at later stages (after 2 kyr) while ascending magma has settled in the vertical conduits/channels and has sufficiently cooled.

5.2 Case 2.

These experiments (Figure 5) correspond to another softening mechanism, where controlling parameters are chosen as follows: $\varepsilon_0 = 0.1$, $\varepsilon_1 = 1.0$, $\lambda = 0.99900$. Reduction in viscosity is thus similar to the previous experiment, but the range of the accumulated strain values, for which progressive softening is applied, becomes larger. In other words, the upper

crust becomes weaker with time than in the previous experiment. It follows that the surface uplift observed before is smaller in these experiments, as can be seen from Figure 5. However, pattern of fracturation, which is actually determined by dynamics of ascending magma, remains relatively similar, consisting in regularly spaced channels of high strain rates (Figure 5). In that case, the funnel-shape structure is not observed, but two Y-shaped structures are present at both edges of the channel tip. These Y-shaped channels differ from conjugate fault zones in the crust, since they could be characterized by larger distance between two branches, by larger vertical size and potentially smaller width, and could also be called, in that case of Figure 5, “U-shaped” structures. It can also be mentioned that topography shows a slight subsidence at the top of each channel, resulting in an undulated surface topography over 100-150 km.

5.3 Case 3 and 4.

The experiments shown in Figures 6a and 6b correspond to another softening mechanism, where controlling parameters are chosen as follows: $\varepsilon_0 = 0.2$, $\varepsilon_1 = 2.0$, $\lambda = 0.99999$ (meaning that the reduction in viscosity reaches a factor of 10^5). The range of strains where softening is applied is thus ~ twice wider than that in previous experiments. This results in a formation of a volcanic-like structure, where deep magma erupts at the surface. Figure 6a corresponds to a tension cut-off value of 10 MPa and Figure 6b shows the case of a tension cut-off value of 1000 MPa. Fractured zones can be inferred from step-like aspects of crustal layers.

5.4 Case 5.

In Figure 6c, controlling parameters are $\varepsilon_0 = 0.2$, $\varepsilon_1 = 0.75$, $\lambda = 0.99900$ and tension cut-off equals 1000 MPa (no Griffith’s criterion). Here again, fracture zones can be easily seen with step-like structures in crustal layers (see inset of Figure 6c). Magma reaches the upper crust and fracturing extends over ~100 km.

The three cases shown in Figure 6 do not illustrate Alaskan-type structures since at the lower crust level, the width of the magmatic channel has been enlarged up to 30-40 km. Contrarily to case 2 (shown in Figure 4) there is, for these 3 cases, no mechanical barrier

above which high strain rate zones would become distributed at the surface over 100-150 km. The following tests show additionnal Alaskan-type structures which were obtained while controlling parameters (ε_0, ε_1, λ and T_0) were varied.

5.5 Case 6 and 7

Figure 7 shows two additional experiments where controlling parameters are respectively: ε_0 = 0.2, ε_1 = 1.0, λ = 0.99900, and ε_0 = 0.1, ε_1 = 1.0 , λ = 0.99990. The first experiment (Figure 7a) show seven Y-shapes structures, whose “trunks” are separated by 28, 55, 25, 23, 30 and 55 km (av. 36 ± 13 km). The second case (Figure 7b) shows seven cylindrical to funnel-shaped structures, separated by 25, 28, 10, 20, 30 and 32 km (av. 24 ± 7 km). As for cases 1 and 2 (Figures 4 and 5), a single deep magmatic source creates several weakness zones in the upper crust, separated by ~20-40 km, thus simulating the clustering aspect of magmatic channels (linear clusters shown in Figure 1).

Contrarily to cases 3, 4 and 5 (Figure 6), where deep material reaches the surface with no apparent mechanical barrier, the other results (Figures 4, 5 and 7) clearly shows at ~20 km depth some drastic changes in the mechanical regime, that favour lateral distribution of high strain rate values.

5.6 Individual bodies

In addition to the reproduction of clustered structures – at least in these 2D numerical models – the obtained geometries of individual weakness zones (or areas with high strain rate values) appear to replicate the schematic models inferred from geological studies, such as the laterally-shifted bodies suggested for Union Bay and Goodnews Bay complexes (Himmelberg and Loney, 1995; Van der Poel and Hinderman, 2000), or the Y-shaped body suggested by Thakurta et al. (2008) for the Duke Island complex. Figure 8 illustrates distinct numerical results of such individual geometries, where it can be seen that dimensions (largely exceeding the resolution limit) correspond to natural cases (see Table 1). Moreover, the amplitudes of the strain rate values (from light green to red delineated by black dashed lines) provide additional information: (1) the strain rate values tend to be higher in funnel-shaped and shallow Y-shaped structures; (2) these zones are located near the bottom parts

of inclined edges. When there are no inclined edges at shallow (~5-10 km) depths, i.e. for vertical pipes such as the two left ones of Y- (or more exactly U-) shaped structures (middle cases in Figure 8), strain rate values are rather homogeneous within the entire structure.

6. Alaskan-type complexes and their PGE mineralization

6.1 PGE concentration

PGE mineralization in Alaskan-type complexes is mainly associated with chromitites hosted by the dunite core. When compared to dunites, chromite concentrations appear to be significantly enriched in PGE by a factor of ~5-6 (Johan, 2002). As emphasized by many studies, mineralized chromitites from Alaskan-type complexes exhibit PGE concentrations anomalously enriched in iridium and platinum (Figure 9). Indeed, the available data (with few exceptions discussed hereafter) show a typical “M” pattern, the two peaks representing Ir and Pt concentrations (Garuti et al., 1997; Johan, 2002; Augé et al., 2005; Zacarini et al., 2011; Nazimova et al., 2011), whereas, by comparison, mineralized podiform chromitites from ophiolites show a decreasing trend from Os-Ir-Ru to Pt-Pd elements (e.g. Ahmed and Arai, 2002; Büchl et al., 2004; Zhou et al., 2005).

The PGE spidergram of Figure 9a illustrates this “M” pattern, as defined by typical mineralized chromites from Alaskan-type bodies. Spidergram of Figure 9b gathers other data which can be considered as coming from anomalously mineralized chromites (either an excess in Os or Pd, or an anomalously low signature in Pt). The Nizhny Tagil 3 and 4 samples correspond to chromitites of barren type and brecciated chromitites, respectively (Augé et al., 2005). Sample from the Butyrin vein in the Kytlym complex shows high concentrations of Os and Pd, while the two other samples (Kytlym 2 and 3) exhibit only slight anomalous Os concentrations and are thus not considered as anomalously mineralized. It is interesting to note that the distribution from the largest Alaskan-type body (the Guli massif, whose total area is around 2000 km², including two dunite cores covering 450 km²), exhibit the lowest Pt concentration with relatively high values for Os, Ir and Ru (Figure 9b). Malitch et al. (2002) also underlined that the common occurrence of Os-Ir-Ru alloys in chromitites

from the Guli massif matches with patterns obtained with ophiolitic massifs. This fact suggests that body size and mineralization features may be related. Another similar observation is described below.

Using geometrical classification described in section 2, the above PGE concentrations from typical mineralized chromites of Alaskan-type bodies (Figure 9a) have been separated in two groups defined by the number of dunite cores (Figure 9c and 9d). It turns out that single dunite cores (Figure 9c) show the lowest ranges of PGE concentrations (curves are located in the lower part of the M pattern area). Figure 9d gathers data from only twin Alaskan-type bodies, and include all the highest PGE concentrations. Note that data from the Uktus 2 sample, which may belong to Figures 9c or 9d (due to uncertainty in the initial number of dunite cores), do not alter this observation.

6.2 Inclined edges

Bottom parts of funnel-shaped ultramafic bodies (not necessarily of Alaskan-type) often correspond to mineralized areas (see discussion). Indeed, these high strain rate zones may concentrate magma pathways, thus enhancing potential for mineral deposition. These high strain rate zones (see section 5.6 and Figure 8), more frequent at the outer edges of the structure, may also explain the concentrically character of Alaskan-type complexes: in case of multiple magmatic pulses, the ascent of dunite cores would be easily followed by subsequent emplacement of pyroxenites around the dunite core, where high strain rate localized during the first ascent. Some field studies have shown a syn-emplacement deformation localized within the complex periphery (e.g. pyroxenite mylonites associated with dykes along borders of Svetloborsky complex, Urals, Tolstykh et al. (2011); solid-state deformation of the Galmoenan complex during ascent and emplacement, Burg et al., 2009). In addition, syn-emplacement deformation is compatible with a translithospheric mantle diapirism mechanism (Bodinier et al., 2002; Burg et al., 2009).

At a smaller scale, a detailed study of the Nizhny Tagil Complex shows that the Platinum Group Minerals (PGM) are systematically included in (or attached to) chromite crystals and are dominated by Ir alloys and Pt alloys, which explains the shape of the

spidergram in Figure 9a. There is a correlation between the PGE content of a given sample and its chromite content. A model has been proposed to explain this relationship, where early crystalized PGM (platinum-group minerals) will be trapped by chromite. The subsequent concentration and accumulation of chromite crystals will cause the PGE enrichment in chromitites. Study of morphology of chromite concentration in the Nizhny Tagil Complex permitted to propose a genetic model where chromite accumulates in cavities along magma conduit created within the dunite unit (Augé et al., 2005). In this model, the cavities created by physical processes were permanently fed by the magma going through the dunite body, the chromite being accumulated by convective processes (Augé et al, 2005, Fig. 14). Figure 10 illustrates this cavity model in the case of a Y-shaped Alaskan-type complex, with some field examples of different surface signatures of Alaskan-type complexes. It is here suggested that both high strain rate zones and the inclined edges of dunite cores of Alaskan-type complexes favour at a smaller scale magma pathways and thus mineralizing processes within cavities.

7. Discussion and conclusion

Alaskan-type bodies have been classified according to their geometrical features at the surface and to their supposed structure at depth. Clustering of several of such bodies within typical distance of tens to hundreds of kilometres represents a specific observation which was attempted to be reproduced through numerical experiments. Based on the emplacement mechanism defined by the ascent of hot magma from the base of the lithosphere through a dyke-like vertical conduit, numerical models have been performed to test the effect of different parameters (thermal regimes, conduit diameter, and rheological parameters) on the mechanical response of the upper crust. After a series of one hundred high resolution experiments, it appears that the only way to keep a vertical dyke-like conduit, while weakness zones develop in the upper crust, is to consider a strong lower crustal rheology and some particular softening mechanisms, including tensile failure and strong strain dependence, in the brittle and ductile domains.

Using ductile softening rules controlled by minimum and maximum accumulated strain values, a range of “Alaskan-type mechanical responses” have been obtained: (i) cluster of cylindrical and funnel-shaped structures, including laterally shifted bodies, separated by 10-40 km, with topographic uplift (Figure 6); (ii) cluster of cylindrical structures, separated by 10-30 km, possibly connected at depth, with pronounced surface subsidence (Figure 7); (iii) cluster of Y-shape structures, separated by 25-55 km, with no significant erosion/subsidence (Figure 7a), and (iv) cluster of funnel-shaped structures, separated by 10-32 km, with pronounced surface subsidence (Figure 7b).

Because of the restricted 2D numerical procedure, a detailed comparison of geometrical aspects of the clustering process is not feasible. In addition, the 2D Cartesian geometry involves a “dyke-like” conduit rather than a “pipe-like” conduit. Consequently, one could simply observe from our simulations that several separated weakness zones can develop within the upper crust over a distance of 100-150 km.

Besides reproducing individual or clustered weakness zones (Figures 4, 5 and 7), the results shown in Figure 8 raised an interesting question dealing with the apparent relationship between locations of high strain rate values and mineralization features reported in Figure 9. Indeed, supposed Y-shaped geological structures – or twin Alaskan-type bodies (Galmoenan, Goodnews Bay, Kachkanar, etc) show the highest PGE concentrations, and Y-shaped numerical bodies have the highest strain rate values. On the opposite, supposed cylindrical geological structures – or single Alaskan-type bodies (Konder, Nizhny Tagil, Tulameen, etc) have the lowest PGE concentrations, while cylindrical numerical bodies exhibit the lowest strain rate values.

Obviously, the lack of data on Alaskan-type intrusion prevents to go further in the interpretation of this relationship. Nevertheless, scarce examples of syntectonic funnel-shaped mafic/ultramafic intrusions exhibit similar geometrical relationships between both the location of melt injections and ore location (Ni–Cu ± PGE mineralization), and the high strain rate zones. For example, the Variscan Aguablanca gabbronorite intrusion (SW Iberia, Romeo et al., 2008) is a funnel-shaped mafic intrusion emplaced in a major shear zone. The Ni-Cu-

PGE mineralization is hosted by a funnel-like magmatic breccia located in the upper part of the funnel, close to the northern border of the intrusion. The mineralization is related to a final magmatic pulse injected within the shear zone (i.e. in the highest strain rate zone) controlling the mafic pluton emplacement. As a second example, the Permian Huangshandong ultramafic/mafic syntectonic intrusion (SW China, Branquet et al., 2012) is also a funnel-shaped intrusion with a sigmoid map shape emplaced within a major shear zone. Ni–Cu mineralization is located close to the border and to the bottom of the intrusion where several coeval melt injections (magmatic mingling) are located and controlled by the shear zone bounding the syntectonic intrusion. These analogies also suggest a control of high strain rate zones on successive magmatic injections and mineralization location.

The approach used in this study corresponds to a series of large-scale thermo-mechanical numerical models applied to metallogenic issues. It has been demonstrated by several authors that the investigation of magma emplacement mechanisms, and more generally of large-scale geodynamic processes, could bring new insights into the understanding of mineralization processes (e.g. Barley et al., 1998; de Boorder et al., 1998; Guillou-Frottier et al., 2000; Pirajno, 2004; Bierlin et al., 2006; Burov et al., 2007; Tosdal et al., 2009; Begg et al., 2010; Guillou-Frottier et al., 2012; Bertrand et al., 2014). Here, we have studied a peculiar magmatic process that involves thermal and mechanical processes at both large (mantle) and small (crust) scales. At these scales, rock properties spanned a wide range of temperatures and pressures, implying that particular caution had to be paid when rheological properties were assessed.

Since rheological parameters seem to control the way the upper crust is fractured, there is *a priori* no reason to assign a particular geodynamic context (e.g. subduction zone) to Alaskan-type bodies. This is consistent with the distinct geodynamic contexts where they occur (mainly in intra-continental and subduction-related settings). However, water-rich ultramafic magmas are probably more easily stored at the base of a continental lithosphere adjacent to a subduction zone.

The fast ascent of ultramafic magma through the lithosphere, which has been invoked by many authors (e.g. Beck et al., 2006; Chen et al., 2009) has been reproduced with a strong viscosity reduction due to strong strain softening. It can be underlined that our ascent velocity is ~50-100 times higher than in Gerya and Burg's models (2007), whereas effective viscosities remain similar. The role of strain softening in viscosity reduction may thus be critical in the dynamical features of ultramafic magmatism.

Among the several unresolved issues which were presented in the introduction, we did not tackle directly the problem dealing with the restricted age range of Alaskan-type complexes. However, it was shown that the favourable rheological conditions required a strong lower crust rather than a weak and ductile lower crust. The possibility of a strong lower crust would thus exist on Earth for only ~500 Myrs, suggesting that a weak ductile crust was predominant prior to this time.

References

Ahmed, A.H., Arai, S., 2002 Unexpectedly high-PGE chromitites from the deeper mantle section of the northern Oman ophiolite and its tectonic implications. Contrib. Mineral. Petrol. 143, 263-278.

Augé, T., Genna, A., Legendre, O., 2005. Primary platinum mineralization in the Nizhny Tagil and Kachkanar ultramafic complexes, Urals, Russia: a genetic model for PGE concentration in chromite-rich zones. Econ. Geol. 100, 707-732.

Barkov, A.Y., Fleet, M.E., Nixon, G.T., Levson, V.M., 2005. Platinum-group minerals from five placer deposits in British Columbia, Canada. Can. Mineral. 43, 1687-1710.

Barley, M.E., Krapez, B., Groves, D.I., Kerrich, R., 1998. The late Archaean bonanza: metallogenic and environmental consequences of the interaction between mantle plumes, lithospheric tectonics and global cyclicity. Precamb. Res. 91, 65-90.

Barnes, S.J., Boyd, R., Korneliusson, A., Nilsson, L.P., Often, M., Pedersen, R.B., Robins, B., 1988. The use of mantle normalization and metal ratios in discriminating between the effects of partial melting, crystal fractionation and sulphide segregation on platinum-group elements, gold, nickel and copper: examples from Norway. In: Prichard H.M., Potts P.J., Bowles J.F.W., Cribb S.J. (editors) Geo-platinum 87. Elsevier, London, pp 113–143.

Bea, F., Fershtater, G.B., Montero, P., Whitehouse, M., Levin, V.I., Scarrow, J.H., Austrheim, H., Pushkariev, E.V., 2001. Recycling of continental crust into the mantle as revealed by Kytlym dunite zircons, Ural Mts, Russia. Terra Nova, 13, 407-412.

Beck, A.R., Morgan, Z.T., Liang, Y., Hess, P.C., 2006. Dunite channels as viable pathways for mare basalts transport in the deep lunar mantle, Geophys. Res. Lett. 33, L01202, doi:10.1029/2005GL024008.

Begg, G.C., Hronsky, J.A.M., Arndt, N.T., Griffin, W.L., O'Reilly, S., Hayward, N., 2010. Lithospheric, cratonic, and geodynamic setting of Ni-Cu-PGE sulphide deposits, Econ. Geol. 105, 1057-1070.

Bertrand, G., Guillou-Frottier, L., Loiselet, C., 2014. Distribution of porphyry copper deposits along the western Tethyan and Andean subduction zones: Insights from a paleotectonic approach. Ore Geology Reviews, in press.

Bierlein, F.P., Groves, D.I., Goldfard, R.J., Dubé, B., 2006. Lithospheric controls on the formation of provinces hosting giant orogenic gold deposits. Miner. Deposita 10, 874-886, 2006

Bodinier, J.-L., Boudier, F., Dautria, J.-M., Bedini, R.M., Burg, J.-P., Pupier, E., Balanec, J.-L., Efimov, A., Prikhodko,V.S., 2002. The Konder « Anorogenic » Ultramafic Massif (Aldan Shield) : Impact of a Translithospheric Mantle Diapir at the Earth's Surface ? Fourth International Workshop on Orogenic Lherzolite and Mantle Processes, Samani, Hokkaido, Japan, Aug 26 – Sept. 3.

Bosch, D., Bruguier, O., Efimov, A.E., Krasnobayev, A.A., 2006. U-Pb Silurian age for a gabbro of the Platinum-bearing Belt of the Middle Urals: evidence for beginning of closure of the Uralian Ocean, in D.G. Gee & R.A. Spephenson (editors), European Lithosphere Dynamics. Geol. Soc. Mem. 32, 443-448.

Branquet, Y., Gumiaux, C., Sizaret, S., Barbanson, L., Wang, B., Cluzel, D., Guangrong, L., Delaunay, A. 2012. Synkinematic mafic/ultramafic sheeted intrusions: Emplacement mechanism and strain restoration of the Permian Huangshan Ni-Cu ore belt (Eastern Tianshan, NW China). J. Asian Earth Sci. 56, 240-257.

Büchl, A., Brügmann,G., Batanova, V.G., 2004. Formation of podiform chromitite deposits: implications from PGE abundances and Os isotopic compositions of chromites from the Troodos complex. Cyprus. Chem. Geol. 208, 217-232.

Burg, J.-P., Bodinier, J.-L., Chaudhry, M. N., Hussain, S. Dawood, H., 1998. Infra-arc mantle-crust transition and intra-arc mantle diapirs in the Kohistan Complex (Pakistani Himalaya): petro-structural evidence. Terra Nova 10, 74-80.

Burg, J.P., Bodinier, J.-L., Gerya, T., Bedini, R.M., Boudier, F., Dautria, J.M., Prikhodo, V., Efimov, A., Pupier, E., Balanec, J.-L., 2009. Translithospheric Mantle Diapirism: Geological Evidence and Numerical Modelling of the Kondyor Zoned Ultramafic Complex (Russian Far-East). J. Petrol. 50, 289-321.

Burov, E., 2007. Plate rheology and mechanics, in Treatise on Geophysics, G. Schubert (ed.), Elsevier, vol. 6, 99-151.

Burov, E.B., 2011. Rheology and strength of the lithosphere. *Mar. Petrol. Geol*. 28, 1402-1443.

Burov, E.B., Guillou-Frottier, L., 1999. Thermomechanical behavior of large ash flow calderas. J. Geophys. Res., 104, 23081-23109.

Burov, E.B., Jaupart, C., Guillou-Frottier, L., 2003. Ascent and emplacement of magma reservoirs in brittle-ductile upper crust, J. Geophys. Res., **108**, 2177, doi:10.1029/2002JB001904

Burov, E., Guillou-Frottier, L., d'Acremont, E., Le Pourhiet, L., Cloetingh, S., 2007. Plume head – lithosphere interactions near intra-continental plate boundaries. Tectonophysics 434, 15-38.

Burov, E. , Yamato, P., 2008. Continental plate collision, P-T-t-z conditions and unstable vs. stable plate dynamics : Insights from thermo-mechanical modelling, Lithos, 103, 178-204.

Burov, E., Cloetingh, S., 2009. Controls of mantle plumes and lithospheric folding on modes of intra-plate continental tectonics: differences and similarities. Geophys. J. Int., 178, 1691-1722

Burov, E., Francois, T., P. Yamato and S. Wolf, 2012. Mechanisms of continental subduction and exhumation of HP and UHP rocks, Gondwana Research, doi: 10.1016/j.gr.2012.09.010.

Butler, R.F., Gehrels, G.E., Saleeby, J.B., 2001. Paleomagnetism of the Duke Island, Alaska, ultramafic complex revisited. J. Geophys. Res. 106, 19259-19269.

Chen, B., Suzuki, K., Tian, W., Jahn, B., Ireland, T. 2009. Geochemistry and Os–Nd–Sr isotopes of the Gaositai Alaskan-type ultramafic complex from the northern North China craton: implications for mantle–crust interaction. Contrib.Mineral.Petrol. 158, 683-702.

Chopra, P.N., Paterson, M.S., 1981. The experimental deformation of dunite, *Tectonophysics*, 78, 453-473.

Chopra, P.N., Paterson, M.S., 1984. The role of water in the deformation of dunite. J. Geophys. Res. 89, 7861-7876.

Chopra, P.N., 1997. High-temperature transient creep in olivine rocks. Tectonophysics 279, 93-111.

Connolly, J.A.D., 2005. Computation of phase equilibria by linear programming: a tool for geodynamic modelling and its application to subduction zone decarbonation. Earth Planet. Sci. Lett. 236, 524-541.

Cundall, P.A., 1989. Numerical experiments on localization in frictional materials, Ing. Arch. 59, 148-159.

D'Acremont, E., Leroy, S., Burov, E.B., 2003. Numerical modelling of a mantle plume: the plume head-lithosphere interaction in the formation of an oceanic large igneous province. Earth Planet. Sci. Lett., 206, 379-396.

De Boorder, H., Spakman, W., White, S.H., Wortel, M.J.R., 1998. Late Cenozoic mineralization, orogenic collapse and slab detachment in the European Alpine Belt. Earth Planet. Sci. Lett. 164, 569-575.

De Brémond d'Ars, J., Jaupart, C., Sparks, R.S.J., 1995. Distribution of volcanoes in active margins. J. Geophys. Res. 100, 20421-20432.

Efimov, A.A., Tavrin, I.F., 1978. On genetic unity of platinum bearing dunites of the Urals and Aldan Shield. Doklady Akademii Nauk SSSR 243, 991-994 (in Russian).

Garuti, G., 2005. Chromite-Platinum mineralization in Ural-Alaskan type complexes (with special reference to the Urals and Russian Far East), XVI Congreso Geológico Argentino, La Plata, 20-23 September.

Garuti, G., Fershtater, G., Bea, F., Monterao, P., Pushkarev, E.V., Zaccarini, F., 1997. Platinum-group elements as petrological indicators in mafic-ultramafic complexes of the central and southern Urals: preliminary results. Tectonophysics 276, 181-194.

Garuti, G., Pushkarev, E., Zaccarini, F., Cabella, R., Anikina, E., 2003. Chromite composition and platinum-group mineral assemblage in the Uktus Uralian-Alaskan-type complex (Central Urals, Russia). Miner. Deposita, 38, 312-326.

Gerbault, M., Poliakov, A.N.B., Daignieres, M., 1999. Prediction of faulting from the theories of elasticity and plasticity: what are the limits ? J. Structur. Geol. 20, 301-320.

Gerya, T.V., Burg, J.-P., 2007. Intrusion of ultramafic magmatic bodies into the continental crust: numerical simulation, Phys. Earth Planet. Int. 160, 124-142.

Gibert, B., Schilling, F.R., Gratz, K., Tommasi, A., 2005. Thermal diffusivity of olivine single crystals and a dunite at high temperature: evidence for heat transfer by radiation in the upper mantle. Phys. Earth Planet. Int. 151, 129-141.

Guillou-Frottier, L., Burov, E.B., Milesi, J.-P., 2000. Genetic links between ash-flow calderas and associated ore deposits as revealed by large-scale thermo-mechanical modeling. J. Volcanol. Geotherm. Res. 102, 339-361.

Guillou-Frottier, L., Burov, E., Cloetingh, S., Le Goff, E., Deschamps, Y., Huet, B., Bouchot, V., 2012. Plume-induced dynamic instabilities near cratonic blocks: implications for P-T-t paths and metallogeny. Glob. Planet. Change 90-91, 37-50

Himmelberg, G.R., Loney, R.A., 1995. Characteristics and petrogenesis of Alaskan-type ultramafic-mafic intrusions, southeastern Alaska. USGS Prof. Paper 1564, 52p., 1995.

Huismans, R.S., Beaumont, C., 2003. Asymmetric lithospheric extension: Relative importance of frictional-plastic and viscous strain softening inferred from numerical experiments. J. Geophys. Res., 108, doi: 10.1029/2002JB002026

Johan, Z., Ohnenstetter, M., Slansky, E., Barron, L.M., Suppel, D. 1989. Platinum mineralization in the Alaskan-type intrusive complexes near Fifield, New South Wales, Australia. Part 1. Platinum-group minerals in clinopyroxénites of the Kelvin Grove prospect, Owendale intrusion. Miner. Petrol. 40, 289-309.

Johan, Z., Alaskan-type complexes and their platinum-group element mineralization, 2002. In: The geology, geochemistry, mineralogy and mineral beneficiation of platinum-group elements, J.L. Cabri (ed.), Ed. Canad. Inst. Mining Metall. Petroleum, 669-719, 2002

Keefner, J.W., Mackwell, S.J., Kohlstedt, D.L., Heidelbach, F., 2011. Dependence of dislocation creep of dunite on oxygen fugacity: implications for viscosity variations in Earth's mantle. J. Geophys. Res. 116, B05201, doi:10.1029/2010JB007748.

Korenaga, J., Karato, S.-I., 2008. A new analysis of experimental data on olivine rheology. J. Geophys. Res. 113, B02403, doi:10.1029/2007JB005100.

Malitch, K.N., 1996. Assessment of the platinum potential of clinopyroxenite–dunite massifs. Dokl. Russ. Acad. Sci., Earth Sci. Sect. 347A, 400–404.

Malitch, K., Thalhammer, O.A.R., 2002. Pt-Fe nuggets derived from clinopyroxenite-dunite massifs, Russia: a structural, compositional and osmium-isotope study. Can. Mineral. 40, 395-418.

Malitch, K.N., Augé, T., Badanina, I.Y., Goncharov, M.M., Junk, S.A., Pernicka, E., 2002. Os-rich nuggets from Au-placers of the Maimecha-Kotui province, Russia: a multi-disciplinary study. Mineral. Petrol. 76, 121-148.

Malitch, K.N., Kogarko, L.N., 2011. Chemical composition of platinum-group minerals from the Bor-Uryakh massif (Maimecha-Kotui Province, Russia). Doklady Earth Sciences 440, 1455-1459.

Mei, S., Kohlstedt, D.L., 2000a. Influence of water on plastic deformation of olivine aggregates. 1. Diffusion creep regime. J. Geophys. Res. 105, 21457-21469.

Mei, S., Kohlstedt, D.L., 2000b. Influence of water on plastic deformation of olivine aggregates. 2. Dislocation creep regime. J. Geophys. Res. 105, 21471-21481.

Mogessie, A., Belete, K., 2000. Platinum and gold mineralization in the Yubdo mafic-ultramafic rocks, Western Ethiopia: historical perspective and some new results. Chron. Rech. Min. 540, 53-62.

Murray, C.G., 1972. Zoned ultramafic complexes of the Alaskan type: feeder pipes of andesitic volcanoes. Geol. Soc. Amer. Memoirs 132, 313-335.

Nazimova, Y.V., Zaytsev, V.P., Petrov, S.V., 2011. The Galmoenan massif, Kamchatka, Russia: geology, PGE mineralization, applied mineralogy and beneficiation. Can. Mineral. 49, 1433-1453.

Nixon, G.T., Hammack, J.L., Ash, C.A., Cabri, L.J., Case, G., Connelly, J.N., Heaman, L.M., Laflamme, J.H.G., Nuttall, C., Paterson, W.P.E., Wong, R.H., 1997. Geology and platinum-group-element mineralization of Alaskan-type ultramafic complexes in British Columbia. British Columbia Geological Survey, Bulletin 93.

Nokleberg, W.J., Bundtzen, T.K., Berg, H.C., Brew, D.A., Grybeck, D.K, Robinson, M.S., Smith, T.E., Yeend, W., 1987. Significant metalliferous lode deposits and placer districts of Alaska. USGS Bull., 1786.

Ouillon, G., Castaing, C., Sornette, D., 1996. Hierarchical geometry of faulting. J. Geophys. Res., 101, 5477-5487.

Pettigrew, N.T., Hattori, K.H., 2006. The Quetico intrusions of Western Superior Province: Neo-Archean examples of Alaskan/Ural-type mafic-ultramafic intrusions. Precamb. Res. 149, 21-42.

Pirajno, F., 2004. Hotspots and mantle plumes: global intraplate tectonics, magmatism and ore deposits. Mineral. Petrol. 82, 183-216,

Pirajno, F., Mao, J., Zhang, Z., Zhang, Z., Chai, F., 2008. The association of mafic-ultramafic intrusions and A-type magmatism in the Tian-Shan and Altay orogens, NW China: implications for geodynamic evolution and potential for the discovery of new ore deposits. J. Asian Sci. 32, 165-183, 2008

Poliakov, A.N.B., Cundall, P., Podladchilov, Y., Laykhovsky, V., 1993. An explicit inertial method for the simulation of visco-elastic flow: an evaluation of elastic effects on diapiric flow in two- or three-layers models, in D.B. Stone and S.K. Runcorn (editors), *Flow and creep in the solar system: observations, modelling and theory*. Dynamic Modelling and Flow in the Earth and Planet Series, pp. 175-195.

Romeo, I., Tejero, R., Capote, R., Lunar, R. 2008. 3D gravity modelling of the Aguablanca Stock, tectonic control and emplacement of a Variscan gabbronorite bearing a Ni-Cu-PGE ore, SW Iberia. Geol. Mag. 145, 345-359.

Ruckmick, J.C., Noble, J.A., 1959. Origin of the ultramafic complex at Union Bay, south-eastern Alaska. Geol. Soc. Amer. Bull. 70, p. 981-1018.

Scheel, J.E., Scoates, J.S., Nixon, G.T., 2009. Chromian spinel in the Turnagain Alaskan-type ultramafic intrusion, northern British Columbia, Canada, Can. Mineral., 47, 63-80.

Simonov, V.A., Prikhod'ko, V.S., Kovyazin, S.V., 2011. Genesis of platiniferous massifs in the southeastern Siberian platform. Petrology 19, 6, 549-567.

Slansky, E., Johan, Z., Ohnenstetter, M., Barron, L.M., Suppel, D., 1991. Platinum mineralization in the Alaskan-type intrusive complexes near Fifield, N.S.W., Australia. Part 2. Platinum-group minerals in placer deposits at Fifield. Mineral. Petrol. 43, 161-180.

Su, B.X., Qin, K.Z., Sakyi, P.A., Malaviarachchi, S.P.K., Liu, P.P., Tang, D.M., Xiao, Q.H., Sun, H., Ma, Y.G., Mao, Q., 2012. Occurrence of an Alaskan-type complex in the middle Tianshan massif, Central Asian Orogenic belt: inferences from petrological and mineralogical studies. Int. Geol. Rev. 54, 249-269.

Sutherland, F.L., 1998. Origin of north Queensland Cenozoic volcanism: relationships to long lava flow basaltic fields, Australia. J. Geophys. Res., 103, 27347-27358.

Suzuki, A., Ohtani, E., 2003. Density of peridodite melts at high pressure. Phys. Chem. Minerals 30, 449-456.

Taylor, H.P. Jr., 1967. The zoned ultramafic complexes of southeastern Alaska, Part 4.III *in* Wyllie, P.J., ed., *Ultramafic and related rocks*, New York, John Wiley, pp. 96-118.

Thakurta, J., Ripley, E.M., Li, C., 2008. Geochemical constraints on the origin of sulphide mineralization in the Duke Island complex, southeastern Alaska. Geochem. Geophys. Geosys., 9, Q07003, doi:10.1029/2008GC001982.

Tirel, C., Brun, J.-P., Burov, E., 2008. Dynamics and structural development of metamorphic core complexes, J. Geophys. Res., 113, doi:10.1029/2005JB003694

Tistl, M., Burgath, K.P., Höhndorf, A., Kreuzer, H., Muñoz, R., Salinas, R., 1994. Origin and emplacement of Tertiary ultramafic complexes in northwest Colombia: Evidence from geochemistry and K-Ar, Sm-Nd and Rb-Sr isotopes. Earth. Planet. Sci. Lett. 126, 41-59.

Tolstykh, N.D., Sidorov, E.G., Laajoki, K.V.O., Krivenko, A.P., Podlipskiy, M., 2000. The association of platinum-group minerals in placers of the Pustaya River, Kamchatka, Russia. Can. Mineral. 38, 1251-1264.

Tolstykh, N.D., Telegin, Y.M., Kozlov, A.P., 2011. Platinum mineralization of the Svetloborsky and Kamenushinsky massifs (Urals Platinum Belt). Russ. Geol. Geophys. 52, 603-619.

Tosdal, R.M., Dilles, J.H., Cooke, D.R., 2009. From source to sinks in auriferous magmatic-hydrothermal porphyry and epithermal deposits. Elements, 5, 289-295.

Toussaint, G., Burov, E., Avouac, J.-P., 2004. Tectonic evolution of a continental collision zone: a thermo mechanical numerical model. Tectonics, 23, TC6003, doi:10.1029/2003TC001604.

Van der Poel, W.I., Hinderman, T.K., 2000. Summary report on lode platinum exploration, Goodnews Bay, Alaska. Anchorage, AK, Alaska Earth Sciences.

Van Keken, P., 1997. Evolution of starting mantle plumes: a comparison betwen numerical and laboratory models, Earth Planet. Sci. Lett., 148, 1-11.

Wang, Q., 2010. A review of water contents and ductile deformation mechanisms of olivine: implications for the lithosphere–asthenosphere boundary of continents. Lithos 120, 30-41.

Weinberg, R.F., Podladchikov, Y., 1994. Diapiric ascent of magmas through power law crust and mantle, J. Geophys. Res., 99, 9543-9559.

Yamato, P., Agard, P., Burov, E., Le Pourhiet, L., Jolivet, L., Tiberi, C., 2007. Burial and exhumation in a subduction wedge: Mutual constraints from thermomechanical modeling and natural P-T-t data (Schistes Lustrés, western Alps). J. Geophys. Res. 112, doi:10.1029/2006JB004441.

Zaccarini, F., Garuti, G., Pushkarev, E.V., 2011. Unusually PGE-rich chromitite in the Butyrin vein of the Kytlym Uralian-Alaskan complex, Northern Urals, Russia. Can. Mineral. 49, 1413-1431.

Zhou, M.F., Robinson, P.T., Malpas, J., Edwards S.J., Qi, L., 2005. REE and PGE geochemical constraints on the formation of dunites in the Luobusa ophiolite, southern Tibet. J. Petrol. 46, 615-639.

Figure captions

Figure 1: a) World-wide distribution of Alaskan-type complexes, as defined by previous studies (first number in parentheses); second number in parentheses refers to our definition (one or two dunite core(s) surrounded by clinopyroxenites); b) zoom on particular areas, where clusters of Alaskan complexes have been described. At the small-scale of the bottom left figure (Yubdo area, Ethiopia), individual massifs separated by a few kilometres can be defined.

Figure 2: Examples of 20 Alaskan-type complexes: a) single circular or elliptical morphology; b) twin bodies of similar size and shapes; c) single elongated geometry, and d) other examples of previous cases, and cases with multiples dunite cores.

Figure 3: Numerical models of diapiric ascent of hot magma from the base of the lithosphere through a narrow vertical conduit. a) initial geometry of the model; colours correspond to different material phases and/or markers zones (crust is painted by 4 layers that have different marker colours but same physical properties). From bottom to top of the mantle, distinct phases are shown by different colours (green = deep magma, light blue = deep mantle, light green = mantle lithosphere). The white dashed line delineates the initial magmatic source and the conduit; b) time evolution from bottom to top, in case of a density contrast ($\Delta\rho$)' (see text) of 0.4 and 0.2 (left and right columns, respectively) between magma and mantle. Colours correspond to different material phases; c) Left: example of the implemented density and mineralogy variations when thermodynamic phase changes are fully taken into account (PERPLEX; Connolly, 2005). Right: strain rate field in case of thermodynamically consistent density (at 30 kyr). At this stage, the magmatic channel has been "destroyed" (laterally eroded). The strain rate field illustrates a nearly vertical conduit in the upper crust (upper cut-off is 5 10^{-12} sec^{-1} , real maximal strain rates in the model are on the order of 10^{-10} sec^{-1}).

Figure 4: Case 1 (ε_0 = 0.2, ε_1 = 0.5 , λ = 0.99900). Strong perturbations in the upper crust are due to the uprising of deep ultramafic magma. Note the incipient surface uplift over a lateral distance greater than 100 km. Figures show: a): distinct phases in the model shown by different colours (green = deep magma, light blue = deep mantle, light green = mantle lithosphere, crustal layers from orange to blue, red: re-deposited eroded material); b): strain rate pattern with a zoomed picture on regularly-spaced weakness zones, appearing in green and yellow vertical conduits; c): topography evolution in km.

Figure 5: Case 2 (ε_0 = 0.1, ε_1 = 1.0 , λ = 0.99900). Strain rate pattern, showing regularly spaced fractures (10-30 km) in the upper crust forming channels with diameters of several kilometers. The inset shows negative topographic signatures of crustal fractures/conduits

Figure 6: a): Case 3 (ε_0 = 0.2, ε_1 = 2.0 , λ = 0. 99999) with a tension cut-off value of 10 MPa. Formation of a volcanic like structure; Same colour code as in Figure 4a. b): Case 4 similar to case 3 but with a tension cut-off value of 1000 MPa. A volcanic like structure is obtained while magma reaches the upper crust. Fractured zones can be inferred from step-like aspects of crustal layers; c): Case 5 (ε_0 = 0.2, ε_1 = 0.75 , λ = 0. 99900) with a tension cut-off value of 1000 MPa, where magma reaches the upper crust and where fracturing extends over ~100km width

Figure 7: Strain rate fields (same color code as Figure 5) for two cases where tension cut-off value equals 10 MPa. a) Case 6 (ε_0 = 0.2, ε_1 = 1.0, λ = 0.99900); b) Case 7 (ε_0 = 0.1, ε_1 = 1.0, λ = 0.99990).

Figure 8: Summary of the individual geometries of the obtained crustal conduits: weakness zones, or zones of highest strain rate values are shown with the same color code as Figure

5, and are delineated by white dashed lines. Zones of particularly high strain rate values are emphasized by black dashed lines.

Figure 9: PGE concentrations measured on chromitites, from the following Alaskan-type complexes : Galmoenan (Nazimova et al., 2011), Goodnews Bay (Johan, 2002), Kachkanar (Augé et al., 2005), Konder (Malitch, 1996), Nizhny Tagil (Johan, 2002; Augé et al., 2005), Polaris (Nixon et al., 1997), Tulameen (Nixon et al., 1997; Johan, 2002), Uktus (Garuti et al., 2003), Wrede (Nixon et al., 1997), Guli (Malitch, 1996), Kytlym (Zacarini et al., 2011). Normalization values are taken from Barnes et al. (1988). a) typical signatures of Alaskan-type complexes, defining a “M pattern” (grey area), with highest concentrations in Ir and Pt; b) data from anomalously mineralized chromites (see text); c) data from single Alaskan-type bodies, presenting the lowest concentrations; d) data from twin bodies, gathering the highest values.

Figure 10: Sketch of an Alaskan-type complex with a Y-shape geometry (left), as inferred from our numerical results. Different levels of erosion (dashed arrows) can yield surface signatures typical of distant or close twin bodies, laterally-shifted and circular bodies (natural cases are indicated on the right). At a smaller scale (bottom sketch) PGE mineralization focused at the bottom of inclined edges of dunite cores, where strain rates are the highest. The model of mineralized cavities comes from Augé et al. (2005).

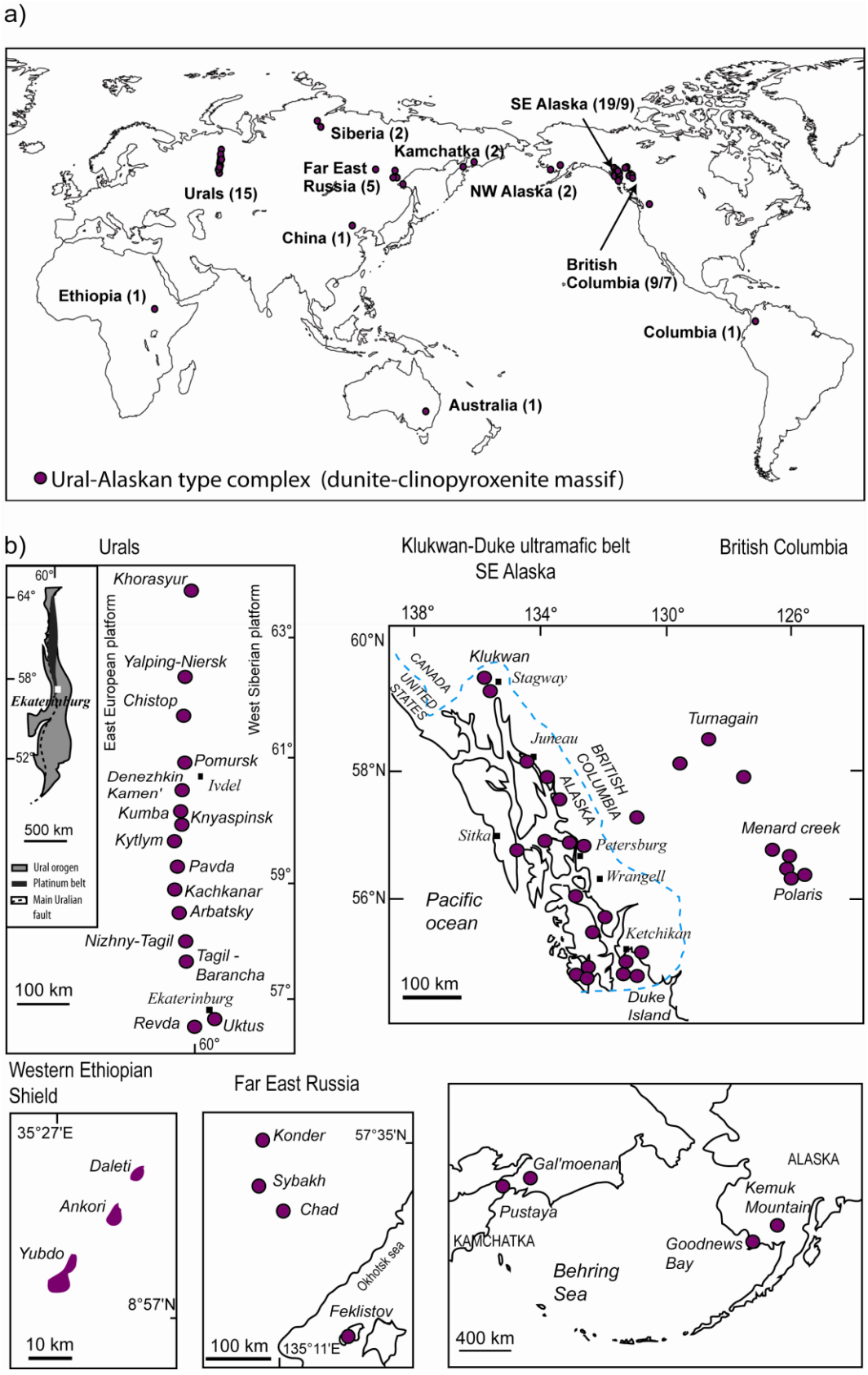

Figure 1

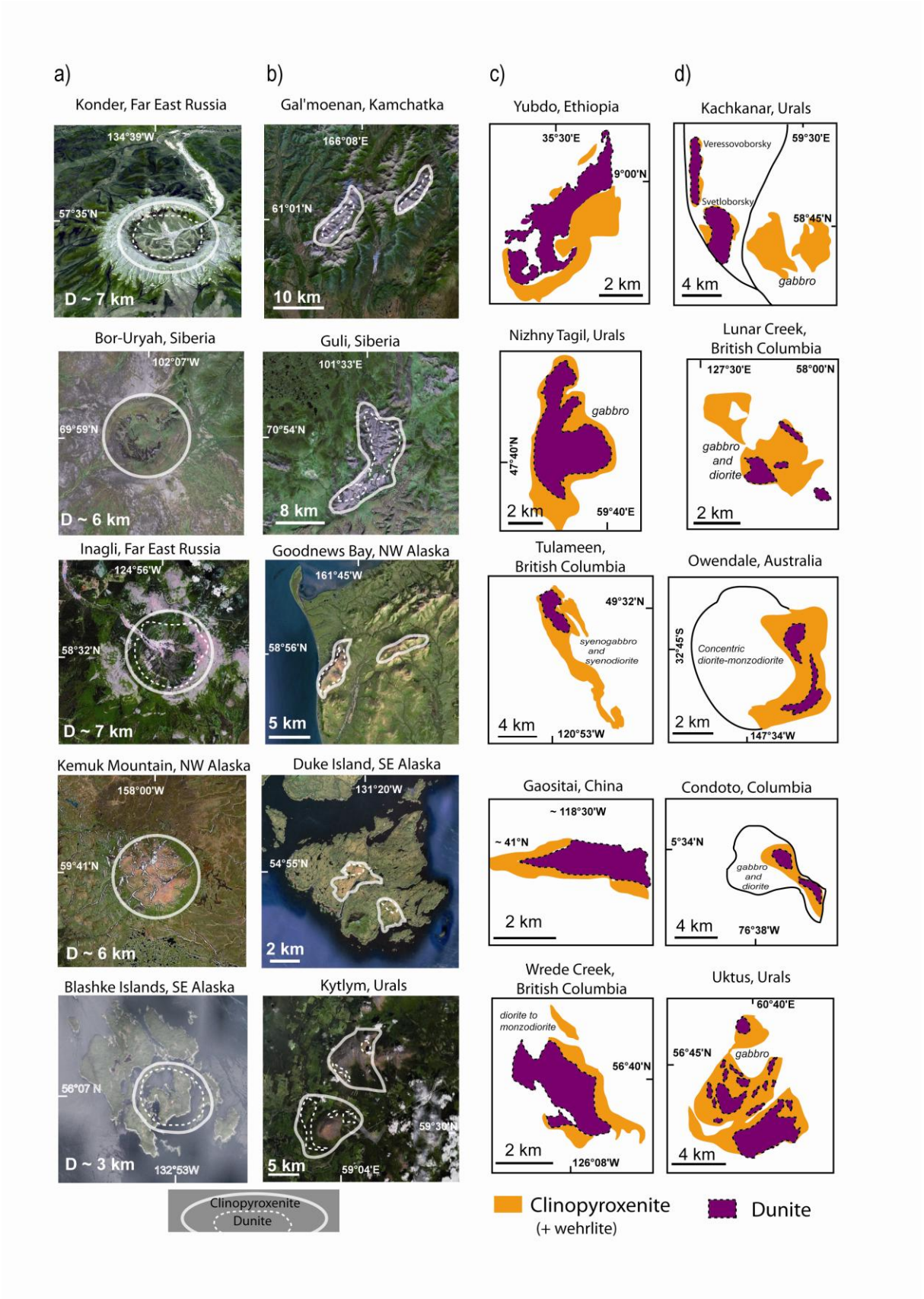
a)
Konder, Far East Russia
134°39'W
57°35'N
D ~ 7 km
Bor-Uryah, Siberia
102°07'W
69°59'N
D ~ 6 km
Inagli, Far East Russia
124°56'W
58°32'N
D ~ 7 km
Kemuk Mountain, NW Alaska
158°00'W
59°41'N
D ~ 6 km
Blashke Islands, SE Alaska
56°07 N
D ~ 3 km
132°53W
b)
Gal'moenan, Kamchatka
166°08'E
61°01'N
10 km
Guli, Siberia
101°33'E
70°54'N
8 km
Goodnews Bay, NW Alaska
161°45'W
58°56'N
5 km
Duke Island, SE Alaska
131°20'W
54°55'N
2 km
Kytlym, Urals
59°30'N
5 km
59°04'E
Clinopyroxenite
Dunite
c)
Yubdo, Ethiopia
35°30'E
9°00'N
2 km
Nizhny Tagil, Urals
gabbro
47°40'N
2 km
59°40'E
Tulameen,
British Columbia
49°32'N
syenogabbro
and
syenodiorite
4 km
120°53'W
Gaositai, China
~ 118°30'W
~ 41°N
2 km
Wrede Creek,
British Columbia
diorite to
monzodiorite
56°40'N
2 km
126°08'W
d)
Kachkanar, Urals
Veressovoborsky
59°30'E
Svetloborsky
58°45'N
4 km
gabbro
Lunar Creek,
British Columbia
127°30'E
58°00'N
gabbro
and
diorite
2 km
Owendale, Australia
32°45'S
Concentric
diorite-monzodiorite
2 km
147°34'W
Condoto, Columbia
5°34'N
gabbro
and
diorite
4 km
76°38'W
Uktus, Urals
60°40'E
56°45'N
gabbro
4 km
Clinopyroxenite
(+ wehrlite)
Dunite

Figure 2

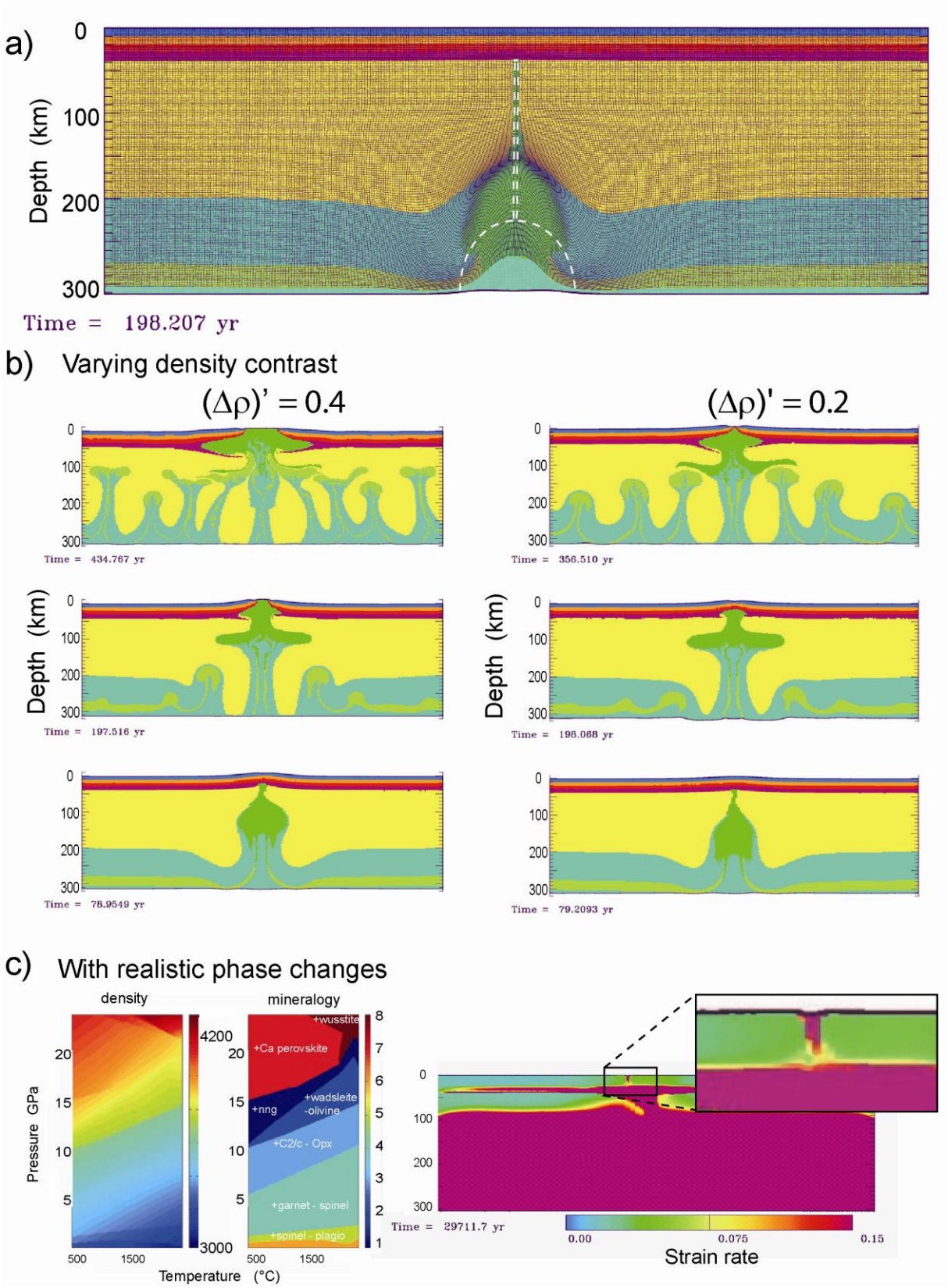
a)
Depth (km)
0
100
200
300
Time = 198.207 yr
b) Varying density contrast
(Δρ)' = 0.4
(Δρ)' = 0.2
Time = 434.767 yr
Time = 356.510 yr
Depth (km)
Time = 197.516 yr
Time = 198.068 yr
Time = 78.9549 yr
Time = 79.2093 yr
c) With realistic phase changes
density
mineralogy
Pressure GPa
4200
3000
+wusstite
+Ca perovskite
+wadsleite
-olivine
+nng
+C2/c - Opx
+garnet - spinel
+spinel - plagio
Temperature (°C)
Time = 29711.7 yr
0.00
0.075
0.15
Strain rate

Figure 3

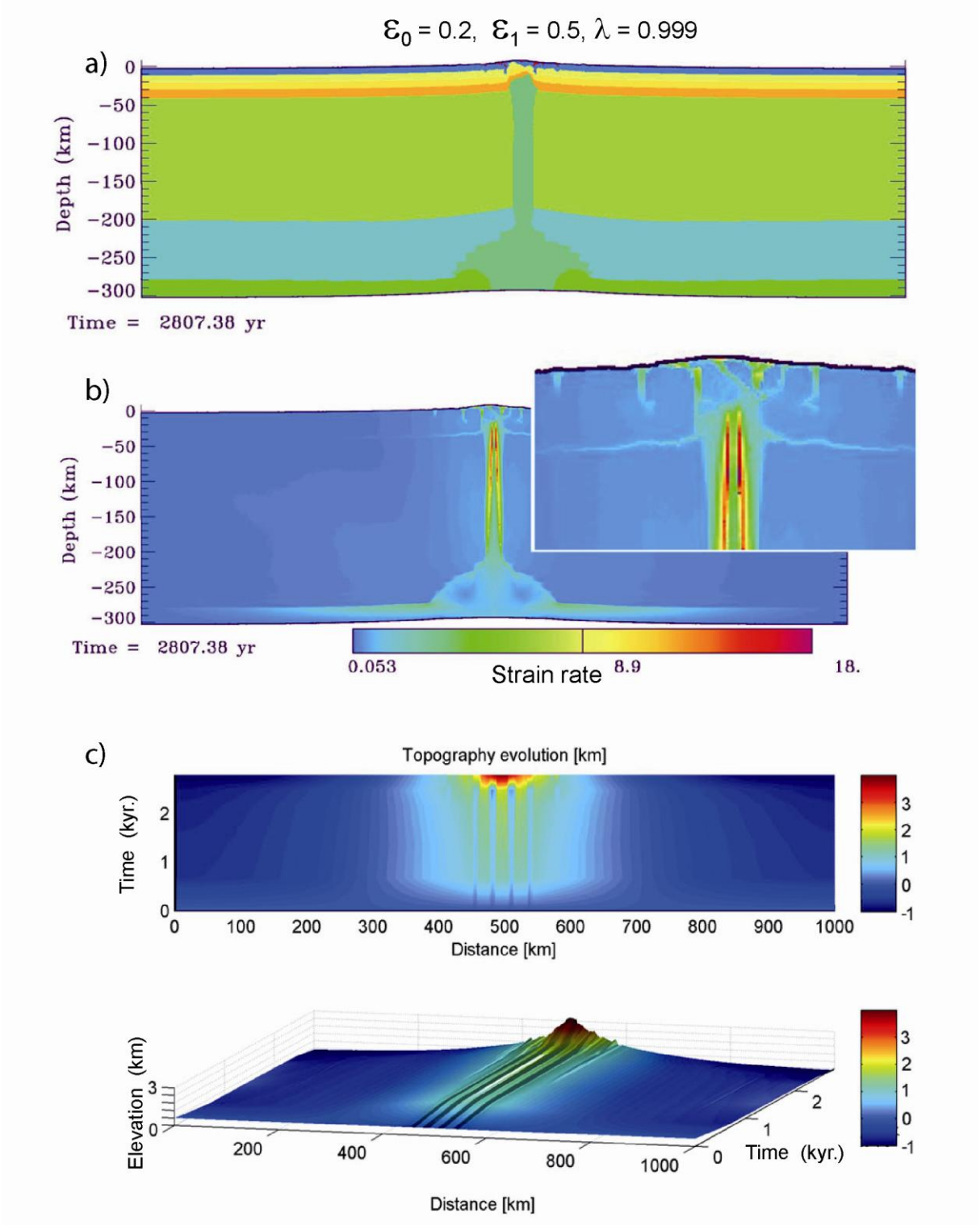

Figure 4

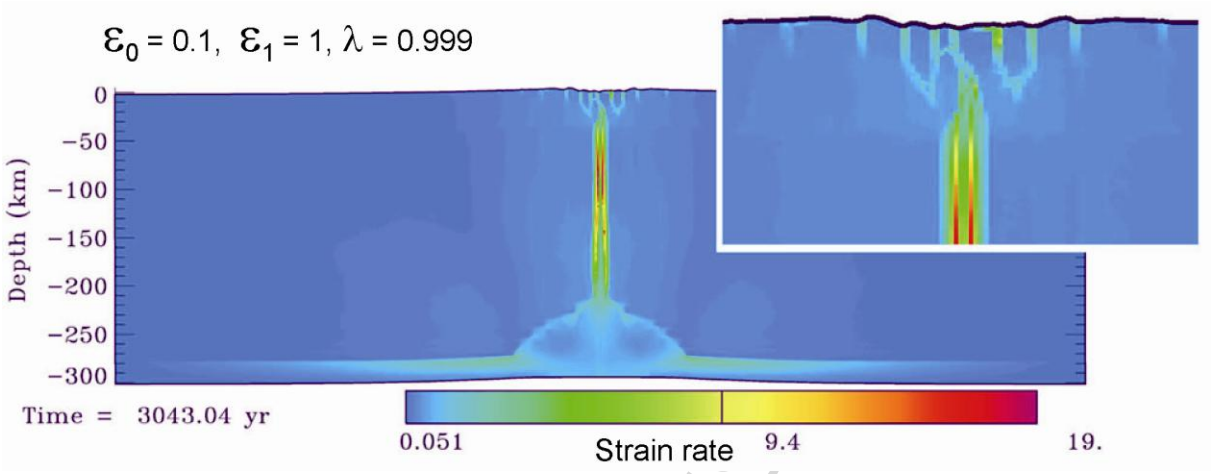

Figure 5

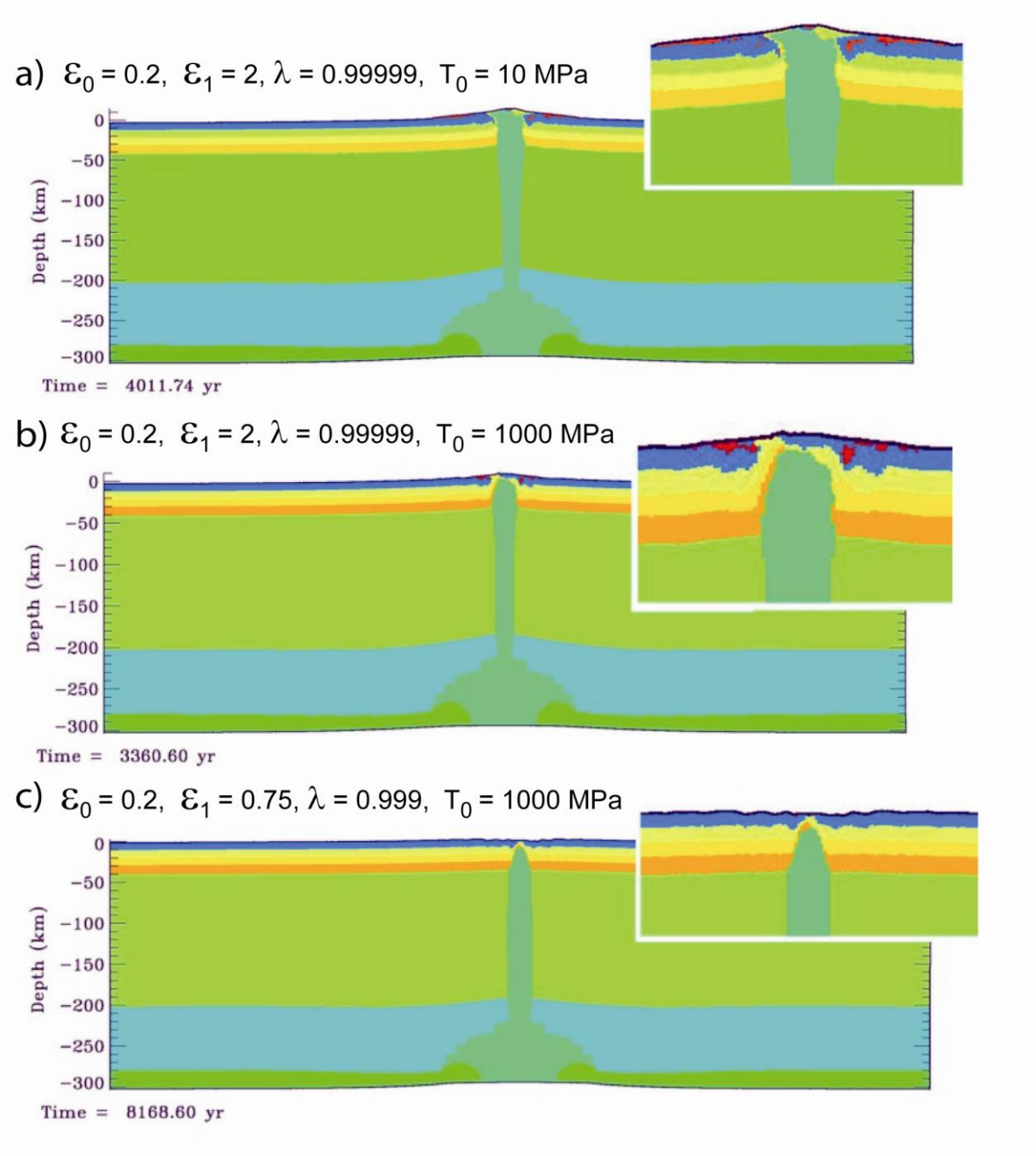
a) ε_0 = 0.2, ε_1 = 2, λ = 0.99999, T_0 = 10 MPa
Depth (km)
0
−50
−100
−150
−200
−250
−300
Time = 4011.74 yr
b) ε_0 = 0.2, ε_1 = 2, λ = 0.99999, T_0 = 1000 MPa
Depth (km)
0
−50
−100
−150
−200
−250
−300
Time = 3360.60 yr
c) ε_0 = 0.2, ε_1 = 0.75, λ = 0.999, T_0 = 1000 MPa
Depth (km)
0
−50
−100
−150
−200
−250
−300
Time = 8168.60 yr

Figure 6

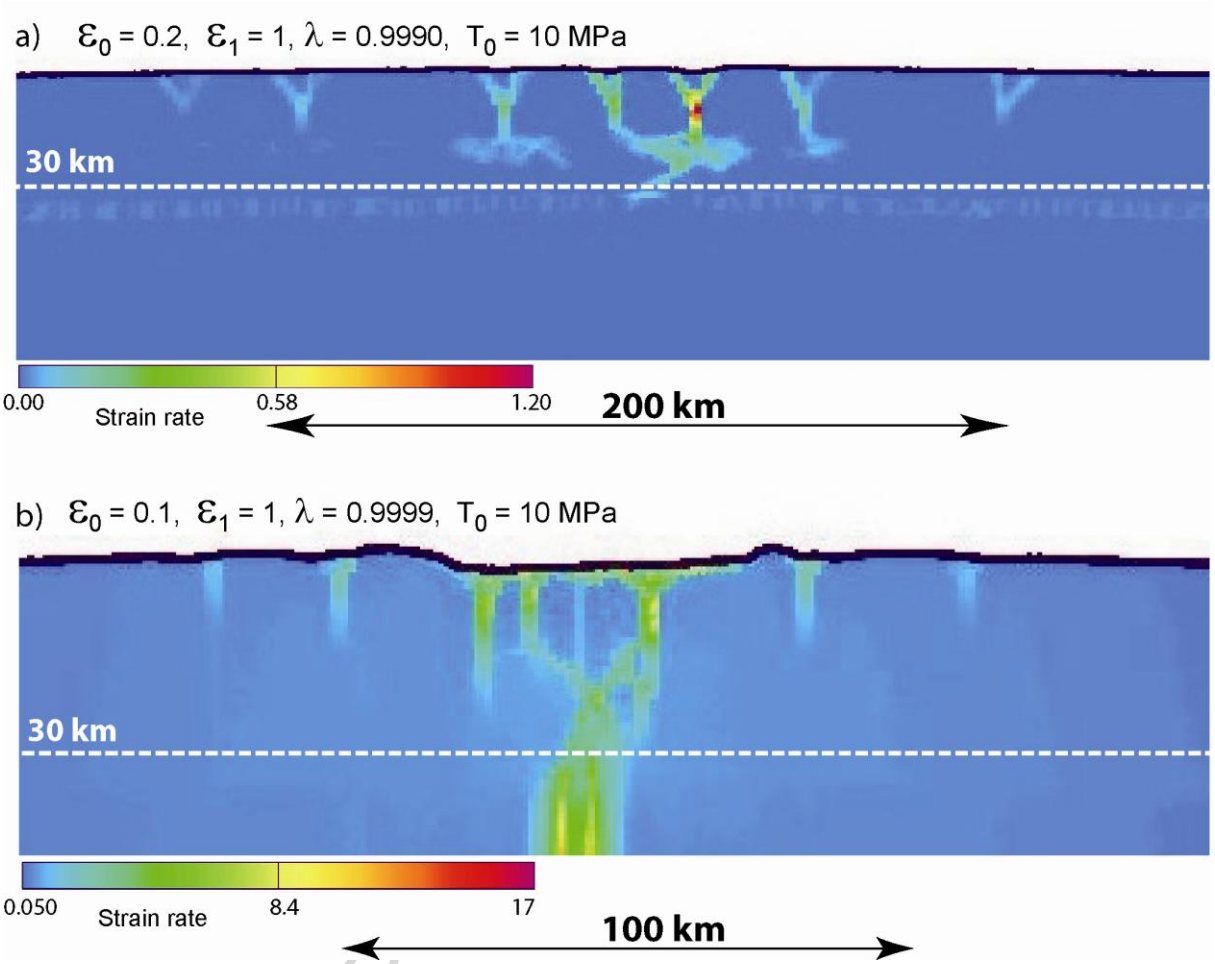

Figure 7

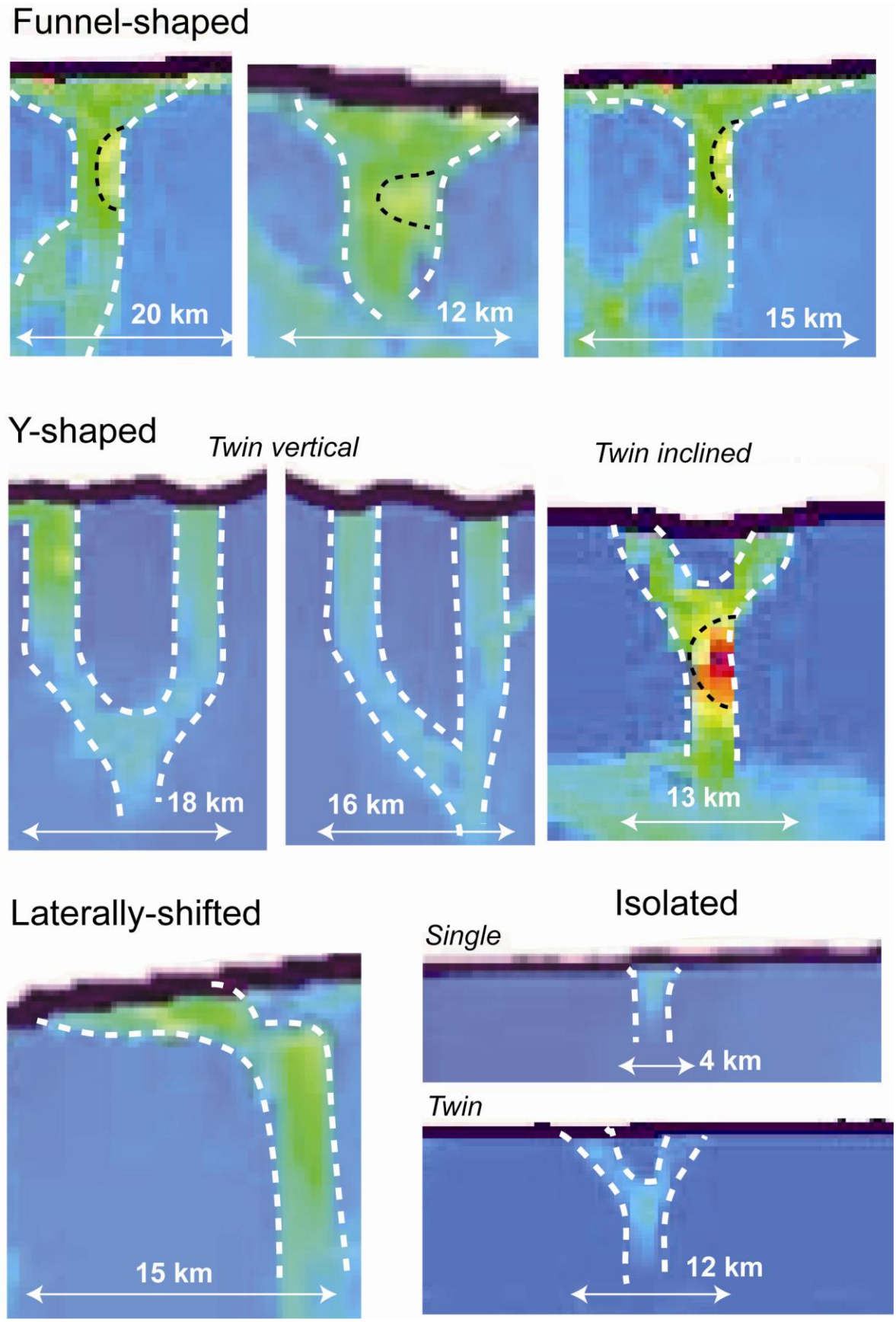
Funnel-shaped
20 km
12 km
15 km
Y-shaped
Twin vertical
Twin inclined
18 km
16 km
13 km
Laterally-shifted
Isolated
Single
4 km
Twin
15 km
12 km

Figure 8

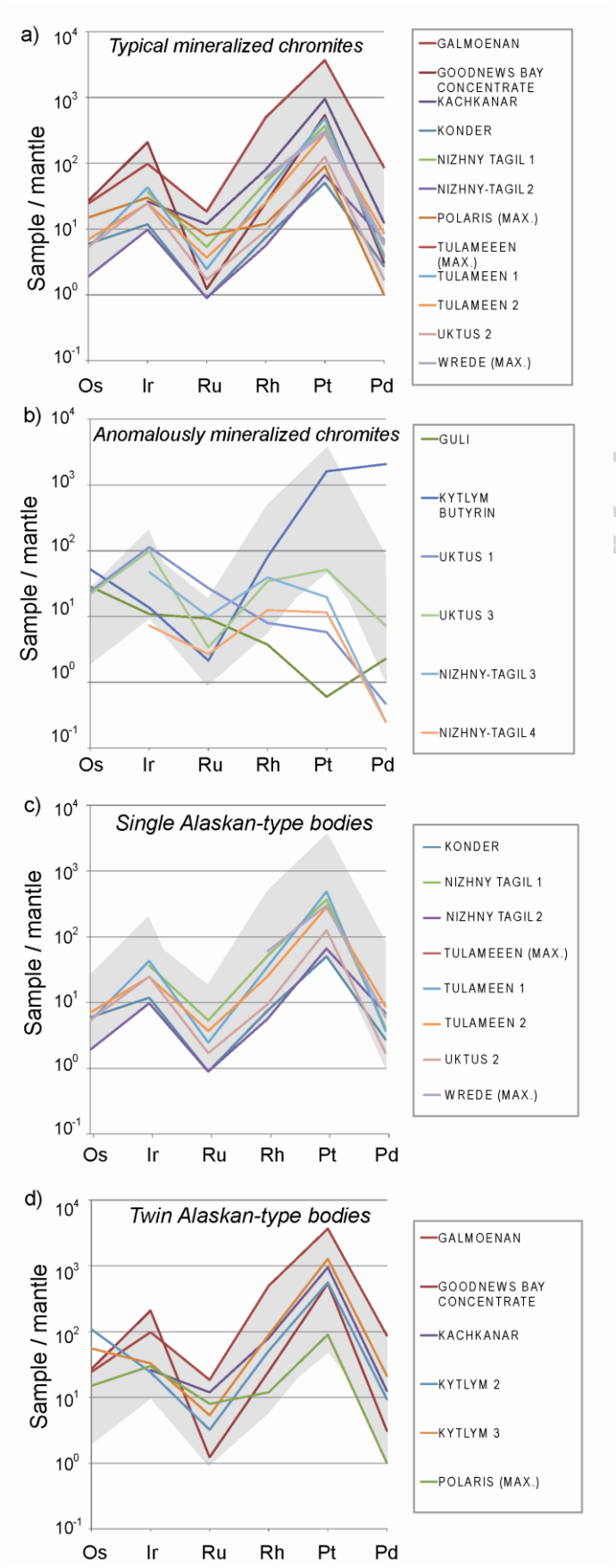

Figure 9

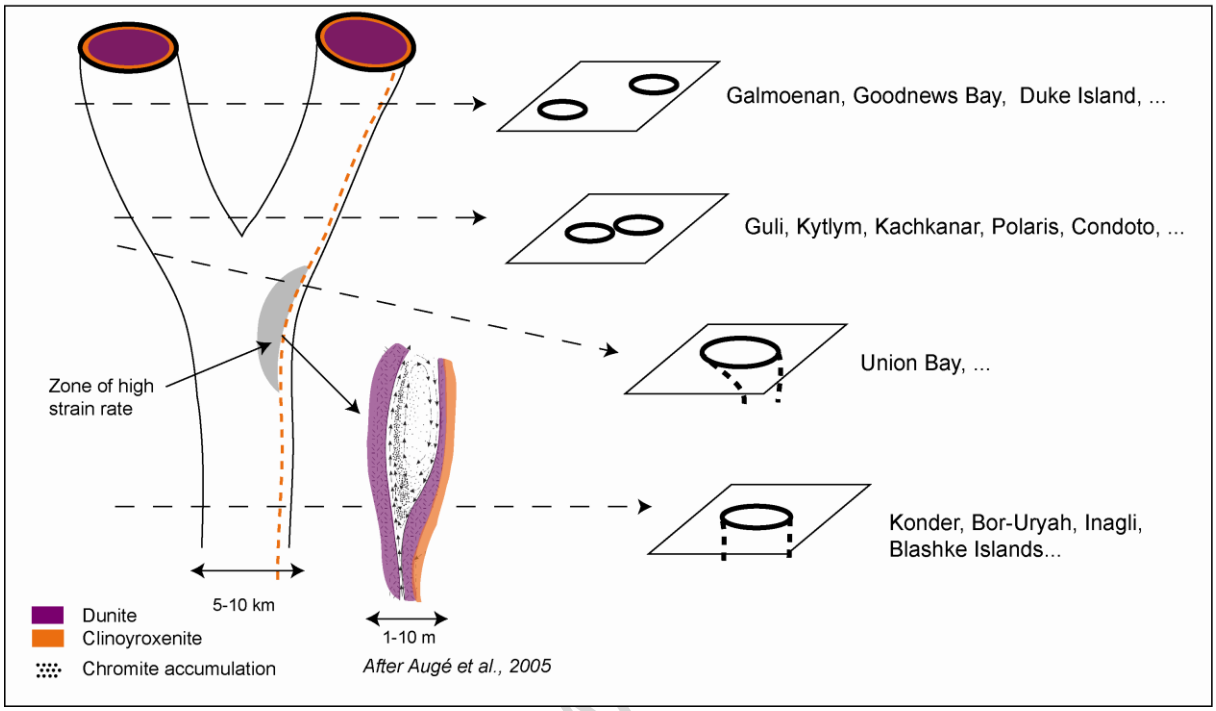

Figure 10

Table 1: List of the 46 Alaskan-type complexes, as defined by dunite-clinopyroxenite massifs.

	Area/country	Site name	Dunite core(s)	LAT	LON	Age (Ma)	Size (diameter, length, or surface)	Mineralization	Reference
1	Urals	Khorasyur		63°30'	60°00'E	415-440	Length ~ 50-100 km		Garuti, 2005
2	Urals	Yalping Niersk		62°00'N	59°55'E	415-440	Length ~ few tens of km		Garuti, 2005
3	Urals	Chistop		61°15'N	59°50'E	415-440	Length ~ 80-100 km		Garuti, 2005
4	Urals	Pomursk		61°00'N	59°56'E	415-440	Length ~ 50 km		Garuti, 2005
5	Urals	Denezhkin		60°20'N	59°52'E	415-440	Length ~ 20 km		Garuti, 2005
6	Urals	Kumba		60°08'N	59°35'E	422-439	Length ~ 15 km		Garuti, 2005; Bosch et al., 2006
7	Urals	Knyaspinsk		59°55'N	59°40'E	415-440	Length ~ 10 km		Garuti, 2005
8	Urals	Kytlym	2 bodies	59°30'N	59°40'E	337±22	725 km²	up to 22972 ppb PGE	Zaccarini et al., 2011; Bea et al., 2001
9	Urals	Pavda		59°15'N	59°45'E	415-440	Length ~ 50 km		Garuti, 2005
10	Urals	Kachkanar	2 bodies	58°45'N	59°30'E	415-440	17 km²; 10 km²	PGE	Augé et al., 2005
11	Urals	Arbatsky		58°15'N	59°30'E	415-440	Length ~ 5-10 km		Garuti, 2005
12	Urals	Nizhni Tagil	Elliptical	57°39'N	59°31'E	415-440	70 km²	PGE	Johan, 2002; Augé et al., 2005
13	Urals	Tagil-Barancha		57°30'N	59°45E	415-440	Length ~ 40 km		Garuti, 2005
14	Urals	Uktus	several bodies	56°46'N	60°51'E	415-440	50 km²	PGE in chromitites	Garuti et al., 2003
15	Urals	Revda		56°46'N	60°05'E	415-440	Length ~ 40 km		Garuti, 2005
16	North Siberia	Bor-Uryah	Circular	69°59'N	102°07'E	215-225	18,5 km²	PGE	Malitch and Kogarko, 2011
17	North Siberia	Guli	2 bodies	70°54'N	101°33E	370	2000 km² (dunite: 450 km²)	PGE	Malitch et al., 2002
18	China	Goaositai		~41°N	~118°30'E	280	4,5 km x 1,5 km		Chen et al., 2009
19	Far East Russia	Inagli	Circular	58°33'N	124°56'E	126; 355	diameter ~7 km	PGE	Malitch and Thalhammer, 2002
20	Far East Russia	Konder	Circular	57°35'N	134°39'E	120; 340	diameter ~7 km	PGE	Malitch and Thalhammer, 2002
21	Far East Russia	Chad		~56°30'N	~135°E			24 ppb Pt	Malitch, 1996
22	Far East Russia	Sybakh	Elliptical	~57°N	~135°E				Johan, 2002
23	Far East Russia	Feklistov	Elliptical	55°N	137°E	115-135	12 km²		Johan, 2002
24	Australia	Owendale	2 bodies	32°43'S	147°28'E	360-415	7 km x 2 km	PGE-Ni; 3400ppb Pt	Johan et al., 1989
25	Kamchatka	Gal'moenan	2 bodies	61°01'N	166°08'E	70-100	14 km x 3 km	PGE	Nazimova et al., 2011
26	Kamchatka	Pustaya	several bodies	~59°N	~162°E	70-100	Placer from bodies	PGE	Tholstykh et al., 2000
27	NW Alaska	Kemuk Mountain	Circular	59°41'N	158°00'W		diameter ~6 km	Fe, Ti, PGE	Nokleberg et al., 1987
28	NW Alaska	Goodnews bay	2 bodies	58°56'N	161°45'W	154-175	6 km x 3 km; 3 km x 1 km	PGE-Au	Johan, 2002
29	SE Alaska	Blashke islands	Circular	56°10'N	132°55'W	*Cretaceous*	10 km²	10-540 ppb Pd; 10-180 ppb Pt	Himmelberg and Loney, 1995; Johan, 2002
30	SE Alaska	Dall island	Circular	54°59'N	132°48'W	400	1-3 km²		Himmelberg and Loney, 1995; Johan,

									2002
31	SE Alaska	Haines	Elliptical	59°20'N	135°35'W	*Cretaceous*	max: 8-10 km		Himmelberg and Loney, 1995; Johan, 2002
32	SE Alaska	Kane Peak	Circular	56°57'N	133°03'W	93-102	7-10 km²		Himmelberg and Loney, 1995; Johan, 2002
33	SE Alaska	Red Bluff	Elliptical	56°51'N	134°49'W	*Cretaceous*	max: 7 km		Himmelberg and Loney, 1995; Johan, 2002
34	SE Alaska	Union Bay	Elliptical	55°47'N	132°02'W	102	11,5 km x 8 km	23 ppb Pd, 93 ppb Pt	Himmelberg and Loney, 1995; Johan, 2002
35	SE Alaska	Annette island	Elliptical	55°06'N	131°26'W	*Cretaceous*	max: 1,5 km		Himmelberg and Loney, 1995; Johan, 2002
36	SE Alaska	Duke island	2 bodies	54°55'N	131°20'W	108-118	5,5 km x 3,2 km; 4 km x 3,2 km	~30 ppb Pt & Pd	Himmelberg and Loney, 1995; Johan, 2002
37	SE Alaska	Percy islands	Circular	54°55'N	131°11'W	*Cretaceous*	24 km²		Himmelberg and Loney, 1995; Johan, 2002
38	British Columbia	Hickman	Elliptical	57°16'N	131°05'W	221-228±16	max: 6 km x 3 km;	Sulphide + gold; low PGE	Nixon et al., 1997
39	British Columbia	Lunar creek	several bodies	57°55'W	127°28'W	237	max: 11 km x 4 km	low PGE	Nixon et al., 1997
40	British Columbia	Wrede creek	Elliptical	56°40'N	126°08'W	219-225	10 km²	PGE in chromitites ; +Cu-Mo	Nixon et al., 1997
41	British Columbia	Johanson lake	several bodies	56°34.5N	126°13'W	232	4 km²	low economic PGE	Nixon et al., 1997
42	British Columbia	Polaris	2 bodies	56°30'N	125°40'W	186	max: 14 km x 4 km; 45 km²	PGE in chromitites; Au	Nixon et al., 1997
43	British Columbia	Tulameen	Elliptical	49°32'N	120°53'W	204-212	8 km x 3 km	PGE in chromitites (8090 ppb Pt)	Nixon et al., 1997; Johan, 2002
44	British Columbia	Turnagain	Elliptical	58°29'N	128°52'W	190	8 km x 3,5 km	Ni-Co, PGE	Scheel et al., 2009
45	Columbia	Alto Condoto	2 bodies	5°34'N	76°38'W	20 Ma	max: 8 km x 4 km	38 ppb Pt	Tistl et al., 1994
46	Ethiopia	Yubdo	several bodies	8°57'N	35°27'E		9 km x 4,5 km	PGE	Mogessie et al., 2000

Highlights

- We numerically reproduced the geometries of Ural-Alaskan-type complexes
- Twin bodies correspond to horizontal cross-sections of Y-shaped structures
- Emplacement and clustering require strong lower crust and strong local softening
- High strain rate zones are located close to inclined edges of Y-shaped intrusions
- Chromite and PGE concentrations are related to geometry and high strain rate zones